ANALYSIS OF ENVIRONMENTAL IMPACTS OF LARGE-SCALE WIND FARMS USING REMOTE SENSING

by

Jenell M. Walsh-Thomas

A Thesis
Submitted to the
Graduate Faculty
of
George Mason University
in Partial Fulfillment of
The Requirements for the Degree
of
Master of Science
Earth Systems Science

Committee:

Guido Cervone	Dr. Guido Cervone, Thesis Director
G. Manca	Dr. Germana Manca, Committee Member
P. Agouris	Dr. Peggy Agouris, Committee Member
P. Agouris	Dr. Peggy Agouris, Department Chair
Timothy C. Born	Dr. Timothy L. Born, Associate Dean for Student and Academic Affairs, College of Science
Vikas Chandoke	Dr. Vikas Chandoke, Dean, College of Science

Date: Thursday, April 26, 2012

Spring Semester 2012
George Mason University
Fairfax, VA

Analysis of Environmental Impacts of Large-scale Wind Farms Using Remote Sensing

A thesis submitted in partial fulfillment of the requirements for the degree of Master of Science at George Mason University

by

Jenell M. Walsh-Thomas
Bachelor of Science
Marist College, 2010

Director: Guido Cervone, Professor
Department of Geography and Geoinformation Science

Spring Semester 2012
George Mason University
Fairfax, VA

DEDICATION

This is dedicated to my unconditionally loving and supportive parents, Teresa Walsh and Mark Thomas.

ACKNOWLEDGEMENTS

I would very much like to express my immense gratitude to Dr. Guido Cervone, my advisor, for his invaluable guidance and time throughout this thesis process. I also wish to thank my other committee members, Dr. Germana Manca and Dr. Peggy Agouris, for their generous support and valuable time and advice. I also thank Dr. Paul Houser for his time initially discussing my thesis topic with me. I am indebted to Dr. Nigel Waters for suggesting I contact Dr. Cervone regarding my thesis topic as well as my experience with him at *Cartographica*. Last but not least, I would like to thank my parents, Teresa and Mark, for their love and encouragement in everything I do. My Father has shared his awe of science with me since as far back as I can remember. I cannot thank my Dad enough for this gift. I thank my Mother for her willingness to always be there to listen and for being my occasional needed distraction. To all my family, including Thomasina and Clementine (my cats), and friends, your encouragement and support has also been greatly appreciated.

TABLE OF CONTENTS

LIST OF TABLES

LIST OF FIGURES

LIST OF EQUATIONS

ABSTRACT

ANALYSIS OF ENVIRONMENTAL IMPACTS OF LARGE-SCALE WIND FARMS USING REMOTE SENSING

Jenell M. Walsh-Thomas, MS

George Mason University, 2012

Thesis Director: Dr. Guido Cervone

Wind energy is increasingly becoming a prevalent alternative, renewable energy resource as societies worldwide are attempting to reduce their carbon footprint in an effort to mitigate the negative effects of climate change and to compensate for the ever decreasing supply of worldwide fossil fuel sources. There are many benefits to utilizing wind energy due to the lack of pollutant releases in the atmosphere, ocean or soil. Particularly important is the decreased carbon dioxide emissions, which has been associated with mitigating climate change. Wind energy is a renewable resource, it can have a positive economic impact, and there are several locations on the planet that are good candidates for wind energy production. While there are many advantages in harnessing wind energy to produce electricity, the impacts of wind turbines and perhaps more importantly of large scale wind farms on the environment need to be determined and examined in a quantitative way in order to make and support sound decisions on the placement of wind farms as well as the mitigation of any harmful environmental impacts. Any direct

environmental impact of large scale wind farms needs to be investigated because it could impact agriculture, economics, health, society, and technology. Baidya Roy, et al (2004); Baidya Roy & Traiteur (2010); and Baidya Roy (2011), have published a series of manuscripts analyzing data obtained from meteorological towers in conjunction with predictions based on computer modeling and hypothesize that large-scale wind farms produce a measureable effect on ambient air temperature. Collecting in situ data quickly becomes difficult from a practical perspective as the size of the wind farm facility increases because many sensors are needed over a large area. Satellite remote sensing observations are particularly suited to study temperature changes over large areas due to the availability of high resolution measurements over many years. While the hypothesis based on relevant literature review is that wind farms have a measureable impact, the proposed goal of this thesis is to quantitatively assess the environmental impacts of operational wind farms, specifically surface temperature and vegetation, with the potential to expand to other variables, using Landsat and other satellite derived imagery, such as from Terra equipped with a moderate resolution imaging spectrometer (MODIS) or SPOT equipped with a vegetation mapper with 1 km spatial resolution.

CHAPTER ONE: INTRODUCTION

Why it is Important and Worthwhile

Wind energy is increasingly becoming the predominant renewable energy alternative to fossil fuels and its use in generating electricity is an essential component of efforts to decrease carbon dioxide emissions in an attempt to counter the anthropogenic element of the already apparent effects of our changing climate (Wiser et al, 2007). According to global installed wind power capacity statistics compiled by the Global Wind Energy Council (2011), while the US and China leads the effort in terms of total installed capacity, on a per capita basis, Germany far exceeds either country in wind energy production. With increases in the number and scale of operational wind farms worldwide, it is ever more important to examine the effects on the environment of this renewable energy solution. Several recent studies have begun to use computer modeling techniques to simulate the local hydrometeorological impacts of wind farms. Only one complete meteorological field campaign is known to have been conducted that is actually within an operational wind farm in which an increase in surface temperature was observed at night and into the morning hours downwind of the wind farm (Baidya Roy & Traiteur, 2010). Other meteorological data that have been used in various studies related to environmental impacts of wind farms have been acquired from measuring stations near the subject wind farms but not from within the wind farm itself. Current studies in progress are incorporating field campaigns involving the direct collection of measurements in the field involving deployment of ground-based data acquisition systems to continuously gather local meteorological information. Other studies related to environmental impacts of wind farms have centered on one or more avian species as well as various aesthetic characteristics of wind farms and their siting.

After investigating these particular instances and targeting the use of remote sensing techniques as well as data acquisition and analysis employed locating ideal places for operational wind farms, satellite-based remote sensing techniques have significant potential value in studying the impacts of wind farms on the environment. **To the best of my knowledge, this may be the first time remote sensing has been applied to this particular problem of measuring environmental impacts of a large-scale wind farm, more specifically regarding temperature.** This is particularly the case in examining large-scale wind farms where acquisition of significant meteorological data with ground based sensors would be prohibitive from both a practical and cost perspective. To expand upon this, there is a recognized need to further consider and empirically support the predictions of the existing computer based models which identify specific environmental effects and this thesis will aim to also shed light on how this can be accomplished with the application of remote sensing methods. As wind power predominantly becomes the renewable energy source choice, it is increasingly important to determine and understand the environmental impacts such installations and operations will have. With any new technology, it is essential to identify the costs and benefits and be sure these costs and benefits are assessed properly to ensure wind power is the right and truly most sustainable and alternative energy source. Many approaches can be taken to effectively accomplish such evaluation. Satellites and other remote sensing techniques including those that are ground-based play an essential role in this assessment process.

There are multiple methodologies that can be employed in the environmental impact assessment of wind farms including the analysis of field data when available and the use of computer modeling. These analyses can be used in both site and construction planning as well as in the actual impact measurements of a wind farm installation as it becomes operational and grows in capacity. This thesis will demonstrate the utility of satellite derived remote sensing data in such assessments allowing for a cost effective and reliable approach towards optimizing the use and minimizing the impact of existing, planned future wind farm installations.

Environmental Effects of Large-scale Wind Farms

As with any energy resource and man-made structure, wind farms do have an effect on the environment, both positively and negatively. In terms of wind farms as an energy resource, it is renewable and does not emit any amount of air pollution and therefore reduces the need for fossil fuel consumption as well as decreases the amount of CO_2 emitted by fossil fuel burning. Documented environmental impacts, as described below, are relatively minor considering the detrimental effects of fossil fuel consumption, especially in terms of climatic effects. However, considering the increase in wind farm construction and the key role of wind energy production, it remains important to continue to study the environmental impacts of wind farms necessary for optimal wind farm placement, which includes the mitigation of negative environmental effects. Remote sensing techniques and capabilities have been demonstrated in a very practical way as valuable tools in identifying environmental changes.

There have been numerous studies regarding specific environmental effects of wind farms such as those that effect both visual and noise pollution, and wildlife. The abundance of such studies can be said to stem from government-mandated targets for reaching a certain level of renewable energy generation by a defined future date. As wind farms have increased in number and in size in an effort to meet these goals around the world, particularly in Germany and the United States, the concern regarding environmental effects focus on potential changes to both ecosystem and natural scenery characteristics, mainly at a local level. Krewitt and Nitsch (2003) have conducted two case studies in Germany using a GIS-based approach to quantitatively assess such impacts. Their approach for the placement of a wind farm and the analysis of potential environmental impacts takes into consideration specific nature conservation aspects and employs a methodology to address and incorporate the local societal view point in a measureable, quantitative way. The nature conservation constraints include: wind speed; residential/industrial area, streets, and railroad lines; landscape conservation areas; breeding areas; flora-fauna habitat areas; and wind speed distribution in remaining areas (Krewitt & Nitsch, 2003). Their study covered both an inland region within the state of Baden-Württemberg, as well as a coastal region situated in northwestern Germany within the state of Lower Saxony. While using this system to evaluate wind energy potential concomitant with minimizing various environmental impacts, mostly at an ecological/biological level it was determined that the prediction for potential wind energy utilization is a low estimate and therefore the areas have greater potential to produce wind energy, though fuller realization of such potential would directly increase environmental impacts.

Remote sensing techniques have recently been employed to monitor the potential and actual collision mortality of avian species at wind farm sites. Both radar and thermal detection systems have been set up on wind turbines or on wind farm sites to observe avian species as they interact with wind turbines by either avoiding or colliding with these structures. Radar has been used as it allows for continuous and simultaneous sampling of bird movements over expansive wind farms at any time of day and under numerous weather conditions (Drewitt & Langston, 2006). More specifically, X-band and S-band surveillance radars are being used for avian species studies at wind farm sites (Desholm et al., 2006). Some radar detection is effected by rain as well as fog and usually only has a range up to 11 km which is not ideal for tracking birds, but large-scale surveillance radar and tracking radar can be used for these purposes. While radar can track a bird or birds and therefore their behavior around turbines, it cannot be used to measure mortality rates due to shadow caused by turbines and the moving rotors (Drewitt & Langston, 2006). This modality is also better implemented at land-based installations as opposed to offshore-based sites, though there are studies currently attempting to improve on radar technology particularly for use at offshore wind farms in order for it to be a practical method under those special circumstances. In studies testing such methods, marine surveillance radar was found to be more cost effective in comparison with tracking and doppler weather radar and have successfully shown avoidance behavior patterns in the vicinity of wind farms offshore (Desholm et al., 2006).

Thermal detection is also being used to determine the collision rate of birds with turbine blades. “Researchers in Denmark (NERI) have been developing the use of remote Thermal Animal Detection Systems (TADS) using an infra-red video camera in an attempt to record birds flying in close proximity to wind turbines” (Desholm et al., 2006). The infrared camera is mounted directly on a turbine, and has been at the Nysted offshore wind farm. It is aimed upwards towards the rotors and is controlled remotely. While these cameras are able to function in poor visibility and at night, there is a low probability of recording a collision because of the camera’s narrow field of vision. To fix this problem however, multiple cameras are needed to be installed per turbine, which allows for a high intensity study to be conducted. During high or peak migration periods, a single camera per turbine may be sufficient though for a low intensity study (Desholm et al., 2006). The data collected has primary importance in models and can provide estimates for four parameters including near turbine blade avoidance behavior, flight altitude, flock size, and species recognition (Desholm et al., 2006).

While there are numerous other studies that examine both a range as well as more specific and discrete environmental impacts as exemplified in the previous examples, there are not nearly as many studies regarding local metrological impacts, which is the central focus of this thesis. In particular, Baidya Roy et al. (2004) began an investigation to identify, determine and otherwise characterize impacts particularly large wind farms have on local meteorology. Specifically, they used the Regional Atmospheric Modeling

System (RAMS), a regional scale weather atmospheric model to study and quantify the potential impacts in the Great Plains region of the US under average summer conditions. They conclude that a large wind farm slows down the wind at the turbine hub height of approximately 72 m, and eddies were created resulting in an enhanced vertical mixing within the local atmosphere. This reduction of speed results in a warming of surface temperature, a drying of surface air and a reduced surface sensible heat flux. This trend was most pronounced at night and in the early morning hours. It is also noted in the study that the wind farm had little influence on evapotransportation. While others have investigated the effects of wind farms on a global scale (Keith et al., 2004), it is necessary to first study and fully understand the effects at the local or regional level. The study of the problem at a global scale is associated with a larger variability due to the size of the problem domain. Although this research focuses on a specific region, the methodology can be applied to different regions and at different scale, if observations are available, and all other relevant controlling parameters are considered in the analysis.

Sta. Maria and Jacobson (2009) have also considered the environmental effects of large wind farms. Their study focused on the interaction between turbines and the atmosphere and estimated both the global and regional atmospheric energy losses due to these interactions as energy changes in the atmosphere directly affect the weather and climate. The Blade Element Momentum (BEM) theory, which determines the forces, exerted on the atmosphere by individual turbine blades allows the effects of a large wind farm to be sufficiently modeled. The findings using the BEM model concluded that the energy losses due to wind farms are high immediately downwind of wind farms but over large geographical regions, the atmospheric effects are quite small. While sufficient, Sta. Maria and Jacobson (2009) do infer that the BEM model would produce better results if coupled with an atmospheric dynamics model and thus better represent a large wind farm.

Baidya Roy and Traiteur (2010) conducted a study at the San Gorgonio area wind farm, which is an expansive installation in Southern California, to determine and analyze its impact on surface air temperatures. They ran a small meteorological field campaign in which it was discovered that there was a cooling effect during the day and warming effect at night downwind. Subsequently these researchers ran the RAMS to determine if the atmospheric model could replicate the observed near-surface air temperature patterns. RAMS was used in 306 simulations in which similar patterns were observed. These simulations made apparent the relationship between rotor characteristics and the atmospheric boundary layer (ABL) flow. With this finding they further explored, using the model, different rotors and ran the model to determine what the effects may be in order to identify which rotor would best minimize the previously observed temperature effects. This study however was merely done over a short time period, February 2009 through August 2009, which only provides a relatively small snapshot of the environmental effects. Also, to conduct similar studies at other wind farms, meteorological data is not readily or reliably available and therefore costly, ground-based meteorological studies would first need to be conducted in order to have sufficient data to input into models. In addition, meteorological data before the installation and operation of a wind farm is also not readily available making it difficult to derive accurate conclusions comparing the status of the local meteorology before and after wind farm installation and operation.

While the previously described study focused on air temperature, a more recent study also utilized the RAMS model to further identify and elucidate any other hydrometeorological effects which comprise near-surface temperature, humidity and surface fluxes of sensible and latent heat (Baidya Roy, 2011). In addition to each of these components, the study also examined the spatial distance of the impacts within and downwind of the wind farm. RAMS was used to conduct 206 simulations to investigate the impact of wind farms on local hydrometeorology and simulated a rectangular domain of 7 x 3 wind turbines, which represented the wind farm. Sounding data from 21 World Meteorological Organization (WMO) stations in the western United States that collected pressure, temperature, relative humidity, wind speed and wind direction data were used as input to give the model information, which characterizes typical meteorological conditions in the region. One of the key results demonstrated using the model was that in a statically unstable atmosphere, turbulence will mix warm air up and cool air down which leads to a cooling at the surface. Another finding was the change in near-surface air temperature and humidity. The model showed that wind farms lead to a warming of surface air. The size of a wind farm was also further explored in this study using the model, which resulted in demonstrating the strongest impacts on hydrometeorology occurred within the wind farms but was also notable downwind. Remote sensing techniques may offer at least a partial but useful solution to both the lack of readily available meteorological data both prior to and after wind farm installation as well as the more specific effects on surface temperature, hydrometeorology, and vegetation.

Applying Remote Sensing

The Landsat program is the longest running satellite imagery acquiring mission with the first satellite launch, Landsat 1, in 1972. Since then a total of seven satellites have been launched, with six being successful, and each having similar instruments onboard the platform though with each successive satellites modifications and improvements of the instruments were made. **The fifth in the series of the Landsat satellites, Landsat 5, the Thematic Mapper (TM) is notably quite good for environmental studies as it provides seven bands, six in the visible and near infrared and one in the thermal infrared (Campbell, 2006)**. The Normalized Vegetation Index can be derived using the third and fourth bands while the sixth band is useful for land surface temperature analysis. Sobrino et al. (2004) presented three different methods of obtaining land surface temperature from band six: estimating land surface temperature from the radiative transfer equation, using a mono-window algorithm, and using a single-channel algorithm. These models at varying levels rely not only on "at sensor measurement" of brightness temperature but also upon a sometimes complex collection of other measurements such as in situ and Normalized Difference Vegetation Index (NDVI) radio-sounding as well as water vapor emissivity. In the general case such corrections of satellite images are clearly a critical image-processing step in order to provide a more widely applicable derivation of land surface temperature (LST). However it is possible at first pass approximation that is commensurate with the purposes of this thesis to simplify the derivation of LST by making simple and easily verifiable assumptions. Wang and DeLiberty (2005) concluded that atmospheric correction models are not needed on days with extremely low humidity and they found that Landsat thermal bands appear to provide very accurate estimates of surface temperatures without the complexities of atmospheric correction. For the particular set of Landsat images examined, atmospheric correction was found to be not necessary for two winter images with cold, clear conditions and low humidity levels throughout the atmosphere. While more complex model based calculations of LST can be employed given the extremely low humidity generally observed in the region of interest a fairly simple and accepted numerical approximation of LST can be employed as follows: the spectral radiance (L) is calculated to be equaled to the L minimum plus the L maximum minus the L minimum times the digital number (DN) divided by 255 (Equation 1). The spectral radiance is then converted into temperature, in degrees Kelvin, (Equation 2) using the two calibration constants (K_1 and K_2). The final step in this calculation is to covert the degrees Kelvin to degrees Celsius with the well-known temperature conversion formula (Equation 3).

Equation 1. Conversion of the Digital Number (DN) to Spectral Radiance (L)

$$L = LMIN + (LMAX-LMIN) * DN/255$$

Equation 2. Conversion of Spectral Radiance to Temperature in Kelvin (T_K)

$$T_K = K_2 / \ln (K_1/L + 1)$$

Equation 3. Conversion of Kelvin to Celsius

$$T_c = T_K - 273$$

Sun et al. (2010) demonstrated the implementation of this model using ERDAS image processing in a case study in the Pearl River Delta area of China to compute LST. The mono-window algorithm (Qin et al., 2001), which was mentioned above, was used in this particular instance to calculate LST after spectral radiance, brightness temperature, NDVI and Emissivity are calculated from TM. This method allowed them to illustrate the urban heat evolution of the region under study. The spatial temporal model within the Model Maker tool of ERDAS IMAGINE is capable of computing the LST, which allows for analysis of temperature changes over a defined time period. With some similarity, this method can be applied to examining the effects of large wind farms on LST and to independently validate other documented in situ temperature increases that have been shown in computer modeling.

While the primary focus of this thesis is to utilize remote sensing techniques to detect a warming near-surface air temperature trend downwind of a large-scale wind farm, another potential environmental impact of large-scale wind farms will be explored: change in vegetation. This variable will be examined through the use of Landsat 5 TM, more specifically bands 3 and 4, and using requisite vegetation indices. These indices combine multiple spectral values by adding, dividing or multiplying the values to arrive at one determination per image pixel that describes numerically the state of vegetation at the location defined by a specific pixel (Campbell, 2006). In general, high values indicate healthy vegetation while low values indicate unhealthy or a lack of vegetation.

When calculating a vegetation index and determining vegetation trends overtime, a ratioing strategy is applied. Due to the inverse relationship between the absorption of red (TM band 3) light of chlorophyll and the strong reflection of vegetation in infrared (IR, TM band 4) radiation by the mesophyll tissue of the vegetation (Elmore et al., 2000), photosynthetic activity and biomass can be measured. Two primary vegetation indices that will be focused on for this thesis study are the normalized difference vegetation index (NDVI) and soil-adjusted vegetation index (SAVI).

NDVI is the most commonly used vegetation index and is a standard method for determining vegetation greenness of an area and comparing differential vegetation greenness overtime. Equation 4 is the formula used for calculating NDVI when using Landsat 5 imagery.

Equation 4. NDVI

NDVI = (Band 4- Band 3)/(Band 4 + Band 3)

When calculations are made, pixel values can range from -1 to 1, with vegetation values ranging between 0.1 and 0.7 and negative values indicating a lack of vegetation. NDVI has several applications including the examination of growing seasons, estimating evaporation over grassland, monitoring grazing of livestock, urban development, land use studies, and change in vegetation of a region over time (either type or quantity).

SAVI is a vegetation index used to account for and minimize the effect of soil background conditions. This index was developed by Huete (1988) to be used in areas where vegetative cover is low and soil surface is exposed, such as in the case of a desert. The SAVI formula Equation 5 is used specifically with Landsat 5 TM imagery.

Equation 5. SAVI

$$SAVI = [(Band\ 4 - Band\ 3)/(Band\ 4 + Band\ 3 + L)] * (1+L)$$

The formula is very similar to NDVI; however it incorporates a constant called the soil-brightness correction factor, L, into the equation. By incorporating L into the equation, soil background conditions are taken into account. An L of 0 is the equivalent of using the NDVI formula while an L of 1 indicates a barren or no green vegetation area. While the optimal L values differ for varying vegetation amounts, L=0.5 is optimal for a wide range of conditions (Huete, 1988). Similar to NDVI, when calculations are made, pixel derived values can range from -1 to 1, where positive values indicate the presence of vegetation and negative values indicating a lack of vegetation. This index, while developed for ground-based data it successfully minimizes soil background effects when utilizing satellite data (Huete & Warrick, 1990), such as data from Landsat 5 TM.

Scientific Questions to be Answered

This thesis is designed/aims to answer these critical questions:

- Can remote sensing data show that wind farms affect near-surface air temperatures?
- Can remote sensing further validate the model simulation findings of previous studies?

- Can remote sensing techniques further explore/detect trends of other [potential] impacts of wind farms such as a change in local precipitation or vegetation?

CHAPTER TWO: DESCRIPTION OF DATA

Region of Interest

The region of interest that was used in this thesis is the San Gorgonio Pass Wind Farm and surrounding area as defined and depicted in Figure 1. As evident in its name, this installation is located within the San Gorgonio Pass of Southern California. The approximate center of the wind farm in terms of geographic coordinates is: 33°54'21.96"N 116°35'39.11"W (33.9061°N 116.594197°W). The San Gorgonio Pass is defined as the area between the San Bernardino Mountains to the north and the San Jacinto Mountains to the south. The regional climate is classified as arid low latitude desert (hot), or BWh, based on the Köppen climate classification (California Dept. of Fish and Game). As determined through the use of Google Earth's measuring tool, the wind farm covers a roughly square area of approximately of 9 km x 9 km. The wind farm's construction began in the 1981 with the first set of turbines operational in 1982(?). While plans for additional wind turbines are in the works, as of January 2008 the wind farm consists of 3218 turbines, which produce 615 MW (U.S. Dept. of the Interior, 2008).

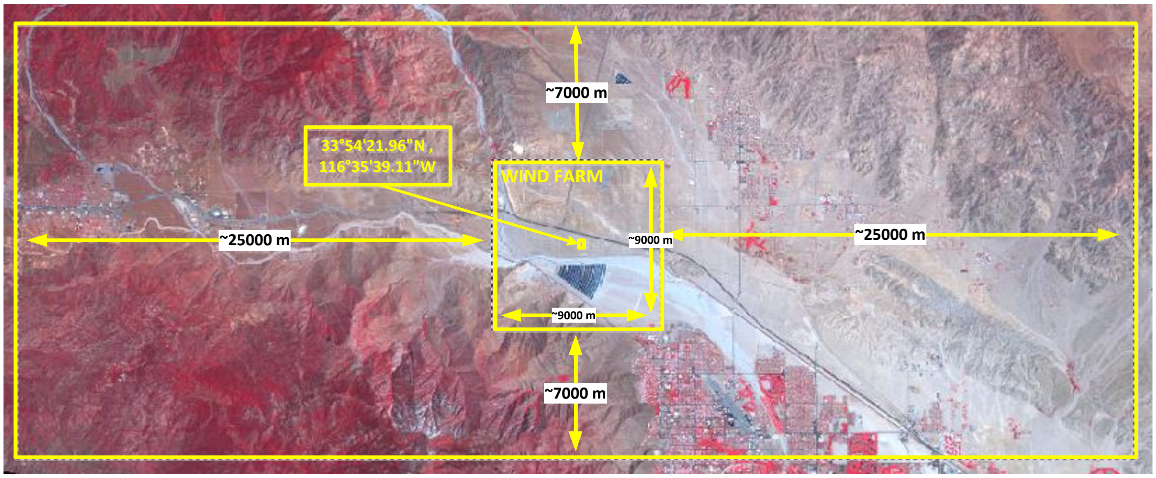

Figure 1. False color composite image of San Gorgonio Pass wind farm and surrounding area of interest for analysis.

Baidya Roy (2011) stated that environmental effects, more specifically hydrometeorological effects as a result of wind farm operation, have been detected 18-23 km downwind of the wind farm. Therefore, the area of interest for analysis purposes has been defined as approximately 25 km outside of the wind farm outer boundary in both east and west directions. The north and south boundaries are delineated as near to 7 km above and below the wind farm outer boundary. The rectangular analysis region boundaries have been approximated using measurement tools in ERDAS IMAGINE with the center of the analysis area being the previously stated center of the wind farm (Figure 1). This rectangular region encompasses a significant area both upwind and downwind of the wind farm which is deemed necessary for subsequent analysis.

Region of Interest: Vegetation Description

The San Gorgonio Pass is located in the Mojave Desert between Mount San Gorgonio in the San Bernardino Mountains and Mount San Jacinto in the San Jacinto Mountains. The mountain peaks directly surrounding the pass are over 10,000 feet in height, (Holtzclaw, 2006) each with diverse vegetation which is strongly influenced by elevation. Each image that has been evaluated has included both the mountain pass itself and portions of Mount San Gorgonio and Mount Jacinto. Here the vegetation present is notable and includes California Black Oak and Coulter Pine as elevation increases (National Park Service, 2006). The arid conditions of the mountain pass provides an ideal environment for hard desert plants which primarily includes low and widely spaced shrubs and are all endemics (National Park Service, 2006). The plants of the Mojave Desert that are found in the San Gorgonio Pass area include the Joshua tree, Parry saltbush, Mojave sage, white bursage and a widely distributed plant, the creosote bush (National Park Service, 2006).

Data Overview

All data for this thesis was obtained from the USGS Global Visualization Viewer (GloVis), specifically from the Landsat Archive collection, Landsat 4-5 Thematic Mapper (TM), resolution 240 m. Landsat 4 and 5 have a 16-day repeat cycle and each maintains a sun-synchronous orbit. The scenes containing the region of interest have a scene center scan time that have a standard deviation of about ± 15 minutes as the orbital node time for Landsat 5 is 9:45 AM ± 15 minutes at the equator. The TM has a seven band system as follows: 1-visible blue, 2- visible green, 3-visible red, 4-near infrared, 5-mid-infrared, 6-thermal infrared (120 m spatial resolution), and 7-mid-infrared (bands 1-5 and 7 have 30 m spatial resolution). This Landsat 5 TM data is being used as it presumptively has more than adequate resolution for the analysis contained herein. An additional practical consideration is that the data is readily available for download and use. The San Gorgonio Wind Farm is in the lower left portion of the identified Landsat scene centered on latitude and longitude coordinates in decimal degrees of 34.6, -116.8; the estimated central coordinate of the wind farm have been previously stated in the above section. At the time of this thesis work and submission, Landsat 4-5 TM scenes are available for download between November 11, 1982 through November 9, 2011; some are available for instant, free of cost download and use, while others must be ordered so they can be processed (1-3 days for processing) and then are available to be downloaded.

The earliest date that data is available for this area is November 11, 1982, as Landsat 4 was launched on July 16th, 1982. However, between March 1983 and March 1984 there are no scenes available. It appears that this region was either not scanned during this time period by Landsat 4 and therefore the data is missing or the images from that time period have not been made available by USGS. Landsat 5 was launched on March 1, 1984 so this is a clear indication that the data after this date is from Landsat 5.

Limitations in the Data

The subject wind farm was initially installed and became operational in the early 1980's and perhaps the primary data constraint lies in the fact that appropriate satellite data prior to wind turbine installation is not available. Performing analysis prior to the initial operation date requires images prior to 1980. While this could potentially be done using other Landsat imagery prior to Landsat 4 and 5, it is felt that the resolution of the imagery would place further limitations on such comparative analysis. Despite this limitation, the twenty-nine year data set collected is quite extensive and substantial.

An additional limitation potentially inherent to the data collected is the amount of cloud cover within the scenes containing the region of interest. This was minimized by selecting images in the summer month of June and the winter month of December that had less than 20% cloud cover. In instances where cloud cover was greater than 20% in the months of June and December, the next available image, +/- two months, with cloud cover was chosen. There were two instances where no image was selected due to high cloud cover percentages. Attention to detail in terms of geographically where the cloud cover occurred in the scene was important as cloud cover directly over the region of interest also made the scene not usable as cloud cover does not allow for accurate surface temperature determination for the pixels affected by cloud cover. Also, the region of interest is only observed about twice per month due to the satellite's orbital parameters so data for every day is not available.

Data Acquisition

Scenes were selected based on availability, observational quality, and cloud cover (≤ 20%). The following table (Table 1) details the dates for each scene used in the analysis:

Table 1. GloVis Scene Acquisition: dates and cloud cover (%) details.

Data Set	Scene Acquisition Date			Cloud Cover (%)
	YYYY	MM	DD	
Landsat 4-5 TM	2011	11	09	2%
Landsat 4-5 TM	2011	06	18	0%
Landsat 4-5 TM	2010	07	01	0%
Landsat 4-5 TM	2009	11	03	0%

Landsat 4-5 TM	2009	06	28	0%
Landsat 4-5 TM	2008	11	16	1%
Landsat 4-5 TM	2008	06	25	0%
Landsat 4-5 TM	2008	01	17	0%
Landsat 4-5 TM	2007	06	23	9%
Landsat 4-5 TM	2007	02	15	0%
Landsat 4-5 TM	2006	06	20	0%
Landsat 4-5 TM	2005	11	24	1%
Landsat 4-5 TM	2005	06	01	5%
Landsat 4-5 TM	2004	12	23	20%
Landsat 4-5 TM	2004	06	14	0%
Landsat 4-5 TM	2003	10	18	19%
Landsat 4-5 TM	2003	06	28	0%
Landsat 4-5 TM	2002	12	18	0%
Landsat 4-5 TM	2002	05	24	0%
Landsat 4-5 TM	2001	11	13	10%
Landsat 4-5 TM	2001	06	06	0%
Landsat 4-5 TM	2000	12	28	0%
Landsat 4-5 TM	2000	06	19	0%
Landsat 4-5 TM	1999	12	26	0%
Landsat 4-5 TM	1999	06	17	0%
Landsat 4-5 TM	1998	12	23	0%
Landsat 4-5 TM	1998	06	30	0%
Landsat 4-5 TM	1997	12	04	10%
Landsat 4-5 TM	1997	06	27	0%
Landsat 4-5 TM	1996	12	01	0%
Landsat 4-5 TM	1996	06	24	0%
Landsat 4-5 TM	1995	10	12	10%
Landsat 4-5 TM	1995	06	22	0%
Landsat 4-5 TM	1994	10	25	0%
Landsat 4-5 TM	1994	06	19	0%
Landsat 4-5 TM	1993	12	25	10%
Landsat 4-5 TM	1993	06	16	0%
Landsat 4-5 TM	1992	12	06	20%
Landsat 4-5 TM	1992	06	13	10%
Landsat 4-5 TM	1992	01	21	0%
Landsat 4-5 TM	1991	05	26	10%

Landsat 4-5 TM	1990	10	30	0%
Landsat 4-5 TM	1990	06	24	0%
Landsat 4-5 TM	1989	11	12	0%
Landsat 4-5 TM	1989	06	21	0%
Landsat 4-5 TM	1988	10	24	10%
Landsat 4-5 TM	1988	07	20	0%
Landsat 4-5 TM	1987	05	31	0%
Landsat 4-5 TM	1986	11	04	10%
Landsat 4-5 TM	1986	06	13	0%
Landsat 4-5 TM	1985	11	01	0%
Landsat 4-5 TM	1985	6	26	0%
Landsat 4-5 TM	1984	10	13	0%
Landsat 4-5 TM	1984	6	23	0%
Landsat 4-5 TM	1982	12	3	10%

The above scenes were accessed through http://glovis.usgs.gov. Once at the site, the collection designated Landsat Archives, Landsat 4-5 TM was selected. This was followed by selecting the resolution option of 240 m. In order to find the scene that contained the region of interest, the approximate center coordinate of the San Gorgonio Pass Wind Farm was entered into the latitude, longitude entry fields in decimal degrees: 33, -116. This however then produces the image that is centered on the coordinates: 33.2, -115.5 and after careful observation of the scene and comparison with the area where the wind farm is located when viewed in Google Earth, it was determined the region of interest is not in this scene centered on 33.2, -115.5. To navigate to and locate the region of interest, the provided up arrow and the left arrow were each clicked once to navigate to the scene centered on 34.6, -116.8. In this scene, the area of interest containing the San Gorgonio Pass Wind Farm is near the lower right corner of the scene. Once the scene containing the region of interest was determined, the maximum cloud cover was set to 20%.

In order to download the scenes in the table, a USGS Earth Explorer username and password that had previously been created was used to access the cart where the images in Table 1 were sent. From the shopping cart, some images were available for instant download while it was necessary for others to be requested. The requested scenes were available for download within a few hours to a few days. As each scene was made available for download, the "Level 1 Product" was downloaded and saved to a designated folder named to match the date of the scene (YYYY_MM_DD) so they were clearly distinguished from each other. The "Level 1 Product" downloaded a zipped *tar.gz file, which once unzipped contained all seven bands (*.tif), and one *.jpg and two text files. Each GeoTIFF had the following file naming convention: LMppprrr_rrrYYYYMMDD_AAA.XXX (see Table 3 for GeoTIFF Product Naming Convention).

Table 2. GeoTIFF file naming convention (Dept. of the Interior USGS, 2009).

L	=	Landsat
M	=	Mission: 4 = Landsat 4 5 = Landsat 5
ppp	=	Product starting path
rrr_rrr	=	Product starting and ending rows
YYYYMMDD	=	Acquisition date of the image
AAA	=	File type: B10 = Band 1 B20 = Band 2 B30 = Band 3 B40 = Band 4 B50 = Band 5 B60 = Band 6 B70 = Band 7 MTL = L1 metadata GCP = Ground Control Points DEM = Digital Elevation Model
.TIF .txt	=	TIF file extension Only the GCP and MTL files end with .txt (e.g., LMppprrr_rrrYYYYMMDD_MTL.txt)

CHAPTER THREE: METHODOLOGY

Overview

The information included in this chapter concisely describes the methodology involved in the temperature analysis for the region of interest as well as the vegetation analysis (NDVI and SAVI) for the subject wind farm and surrounding region. It is important to note all images from Table 1 were used for the analysis and the same set of images were examined for both land surface temperature and vegetation analyses. A brief overview of the methodology is depicted in Figure 2. As shown in the diagram and discussed in detail below, a second quantitative temperature analysis was used to provide an additional verification of the overall findings of this thesis. Examining the data via multiple techniques has allowed for the unambiguous comparison of the effects of the wind farm upwind vs. downwind to be made accurately, precisely and in a consistent manner.

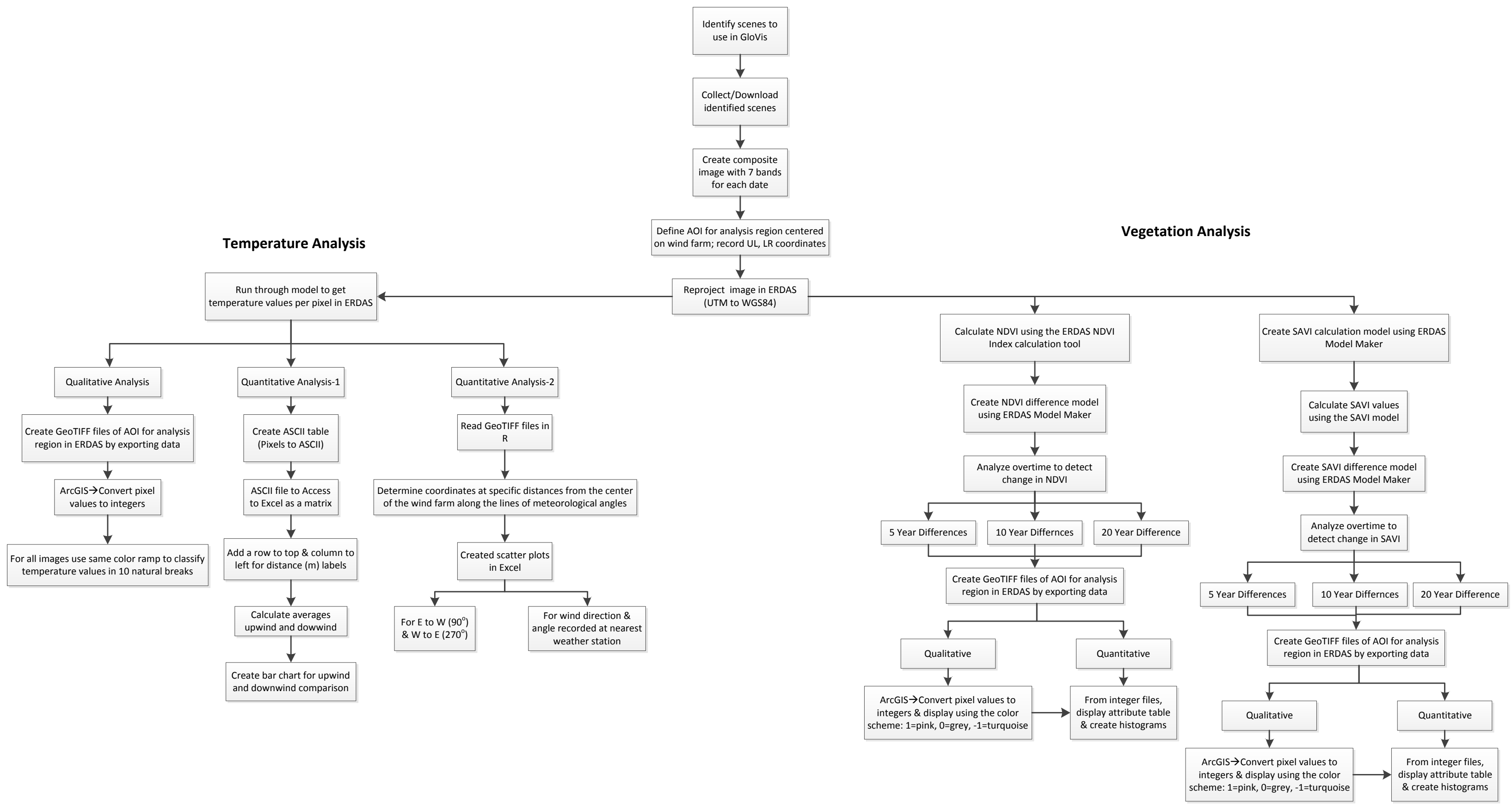

Figure 2. Methodology Summary Flow Chart.

Scene & Image Preparation

Once all appropriate and necessary scenes were collected (Table 1), scene and image preparation was necessary before any analysis could be completed. Scene and image preprocessing included creating a composite image, defining the area of interest (AOI) of the wind farm which involved defining the center of the analysis AOI, defining the boundaries of the analysis AOI, and reprojecting the analysis AOI to WGS 84 coordinates from Universal Transverse Mercator (UTM) notation. Each composite image was created using the data management tools composite image creator in ArcGIS (Figure 3). This process was necessary because the ERDAS model, which was subsequently used to convert the digital number (DN) to a temperature value, required a composite Landsat TM image that contained seven bands with the sixth band being the thermal band.

Measurement tools in ERDAS were used to define all AOIs and the center of the analysis region of interest. The analysis region was determined by measuring 7 km both north and south of the outer boundary of the wind farm area and 25 km both east and west of the outer boundary of the wind farm which created the 59 km x 23 km AOI as depicted in Figure 1. This in turn defined the upper left (UL) and lower right (LR) coordinates of the ROI which are: UL X: -116.64253264, UL Y: 33.94693382; LR X: -116.54569932, LR Y: 33.86622616. The AOIs created encompass a sufficient region both upwind and downwind of the wind farm for analysis. The upper left and lower right coordinates were carefully recorded for use when reprojecting only the analysis AOI from UTM to WGS 84 coordinates which was completed using the reproject tool in ERDAS.

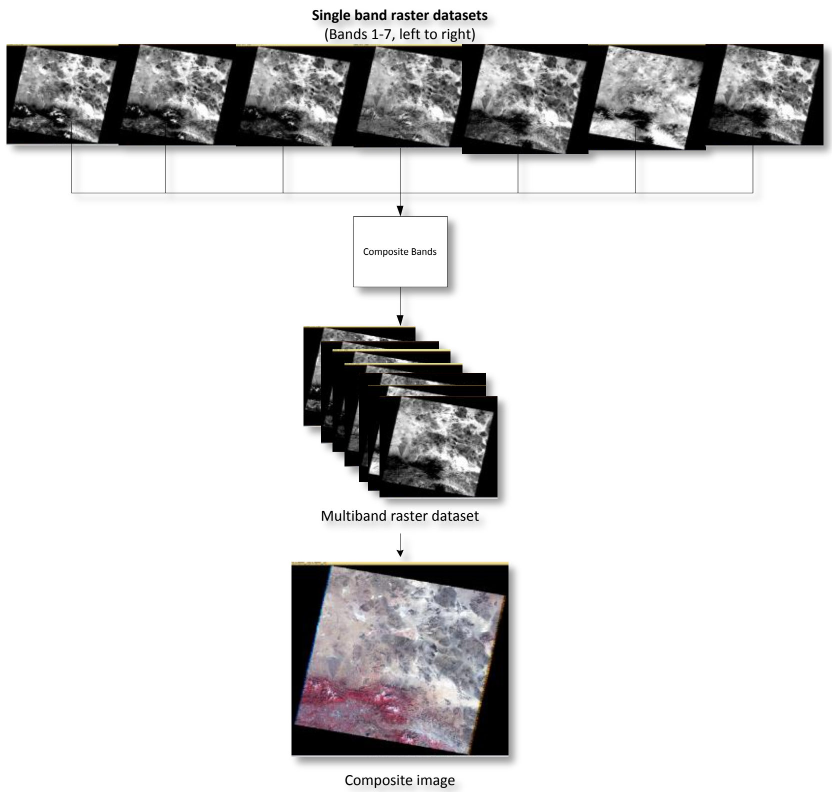

Figure 3. Creating a Composite Image.

Models were also created and used in order to further prepare scenes for both temperature and vegetation analysis. Temperature and vegetation analysis were completed with the facilitation of various tools found in ERDAS and ArcGIS. These tools include those found in the Data Analysis Tools and Spatial Analysis Tools of ArcMap and the Model Maker function and calculation tools found in the Raster tab of

ERDAS. The models and other analysis steps are discussed for temperature and vegetation respectively in more detail below.

Temperature Analysis Methodology

Both qualitative assessment and quantitative analyses were conducted for the ROI. Each image was first run through the temperature model which was created in ERDAS. For the qualitative analysis, GeoTIFF files were displayed in ArcGIS to obtain a temperature variation image. Two, independently executed temperature analyses were performed to provide separate confirmation of LST patterns surrounding the subject wind farm. In the first quantitative analysis, the output images from the ERDAS model were converted to an ASCII file subsequently used to create a matrix of temperature values while in the second quantitative analysis, the GeoTIFF files were read directly into the R statistical computing package and employed the use of meteorological angles and specific wind direction to identify pixels for subsequent analysis.

Landsat TM 5 Temperature Model

With the composite images created and the ROI reprojected in WGS 84, the Model Maker function in ERDAS and a spatial model for converting spectral radiance to temperature values in degrees Celsius from band 6 of scenes from Landsat 4 and Landsat 5 TM data was used to produce a grayscale surface temperature image. In the Model Maker, the graphical model "Landsat_Temperature.gmd" was opened (Figure 4); however, it was necessary to slightly modify it. By double clicking on the first circle, or function, of the model, the maximum spectral radiance value (LMAX) was changed from 15.600 to 15.303. This LMAX value, as well as the minimum spectral radiance (LMIN) value, was found in the header file provided with each image. It was necessary to change this value in order for the calibrated DN to be properly converted to spectral radiance when the model was executed. To run the model, a composite image was selected as the input file and an output surface temperature file was named and created for that specific date. As depicted in Figure 4, the model converts the calibrated DN to spectral radiance and creates a temporary raster which is followed by converting spectral radiance to temperature units in Kelvin and finally converts units in Kelvin to units in Celsius. To confirm the model had run successfully, the newly created output file was opened and selected pixels values were viewed using the Inquire feature in ERDAS.

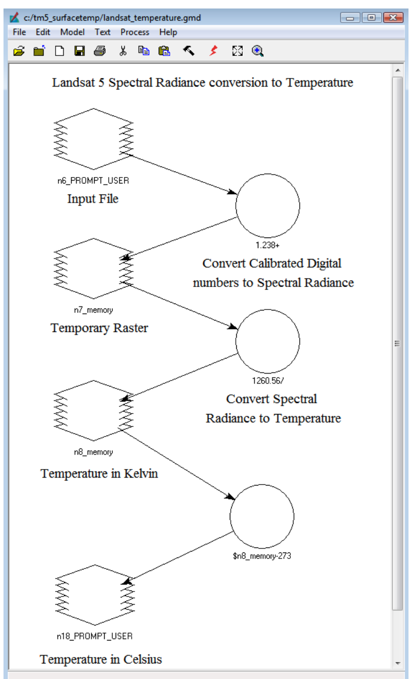

Figure 4. Landsat Temperature Model in ERDAS Model Maker.

Qualitative Analysis

For the qualitative analysis based on visual examination of images, the surface temperature files were exported as GeoTIFF files to be opened in ArcGIS. Using the Spatial Analysis Tool, the pixel values of each image were converted to integers and displayed using a specific color ramp which classified temperature values into ten natural breaks, and each temperature range was an assigned color. Viewing the images in this manner allowed for a visual analysis to be completed and one is clearly able to observe the temperature variation across the region. The outcomes of this procedure are seen in the Chapter 4.

Quantitative Analysis I

The first quantitative analysis was completed to provide further rigor in testing the hypothesis of this thesis as well as support the conclusions drawn based on the qualitative analysis. In order to complete the quantitative analysis, a temperature matrix was created from the pixel values that were calculated from the Landsat 5 TM temperature model. This was completed in several steps largely due to the limitations of working with large ASCII files containing approximately 1.5 million values. In essence, the Excel temperature matrix that was created for each image is a cross tabulation of values contained in an ERDAS *.asc file. An ASCII file was created first using the data management tool in ERDAS which converts pixels within a selected image to ASCII file format; essentially creating a simple linear, three-column table containing X (longitude) and Y (latitude) map coordinates along with associated temperature values. The ASC files exported from ERDAS were edited with a text editor to remove leading header values as well as trailing blank lines placed by ERDAS at the end of each file. This file was then imported into a Microsoft Access table as Excel is incapable of reading in the approximate 1.5 million rows of data. The Access table was then written to a CSV file by using a simple custom macro. The CSV file was then opened in Excel and subsequently annotated as shown in Figure 5. This file was saved as an Excel Workbook for subsequent analysis.

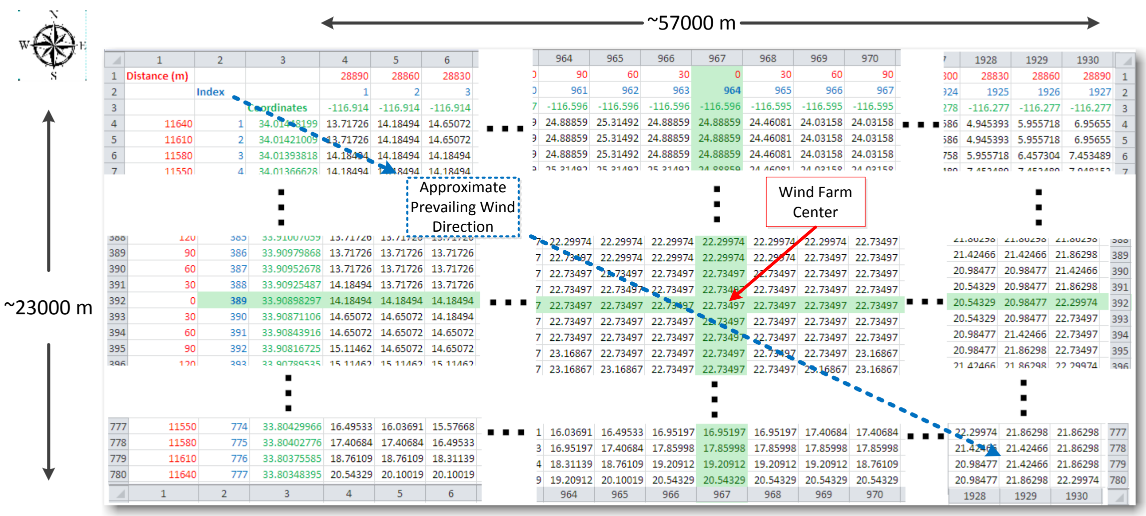

Figure 5. AOI Surface Temperature Matrix.

For convenience in visualizing the analysis, the AOI Surface Temperature Matrix is simply indexed by row and column positions where the row (height) indices are numerically sequenced from 1-777 and the column (width) indices are numerically sequenced from 1-1927. The exact maximum values are simply an artifact of the process in which the standard AOI to be used across all identified image was selected using ERDAS imagine. In the above diagram, each pair of row and column indices represents one pixel of an image. While the Landsat-5 specification states that thermal band resolution is 120 meters per pixel, the other bands which are part of the multi-layered geo-spatial image from which the above matrix is derived provides a resolution of 30 meters per pixel. Hence, each cell of the above matrix provides separate LST value which is simply interpolated from the overlapping 120 meter pixel value. Since one of the primary goals of the proceeding analysis is to assess the LST impact attributable to the presence of the wind farm and to characterize this impact as a function of the distance from the wind farm, the matrix also explicitly contains distances as measured from the X and Y axes which cross the appropriate center pixel of the wind farm itself. This was used as a visual aid to quantify this relationship and for selecting sets of upwind and downwind LST pixel values used in the analysis.

With the latitude and longitude coordinates in the Excel matrix, the values within the wind farm were identifiable and distinguishable from the other cells. Visualizing the boundaries of the wind farm, averages downwind and upwind from the wind farm were calculated using 2 km x 2 km areas, for a total extent of 12 km downwind and 8 km upwind, which are represented in Figure 6. The 2 km x 2 km areas were chosen to avoid observable topographic and elevation impacts on the temperature values being averaged as well as to be consistent with the direction of the mountain pass. The averages were then displayed in bar charts as are shown in the next chapter with each region, 2 km, 8 km, 10 km, and 12 km downwind and an upwind region average displayed respectively as bars and the y-axis showing the temperature in degrees Celsius. From the derived averages, a comparison between upwind and downwind temperatures was then able to be made.

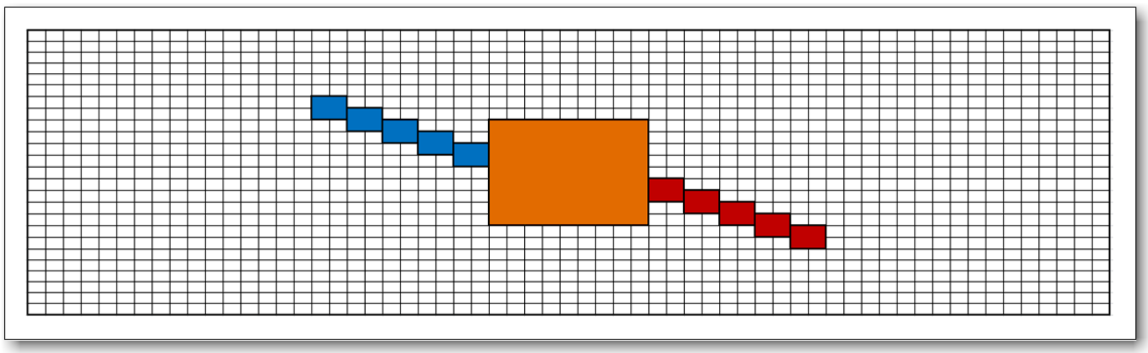

Figure 6. Representative of data analysis areas up and downwind of the wind farm as a function of distance. This depicts the temperature value matrix including the wind farm (orange) and the 2 km x 2 km areas (blue, upwind; red, downwind) where temperature values were averaged.

Quantitative Analysis II

A second quantitative analysis was completed to further validate the findings of both the qualitative analysis as well as the first quantitative analysis. In R, a language and environment for statistical computing and graphics, the GeoTIFF files were read. The center of the wind farm was used as the frame of reference and to define the central coordinate from which to measure the meteorological angles from 0^o to 360^o, in increments of 15^o (Figure 8). Once defined, latitude and longitude coordinates were determined for specific distances along each angle's line from the center in order to acquire the temperature value of the particular pixel at the specified coordinate along each line. These coordinates were defined to identify the temperature values at specific distances upwind and downwind of the wind farm at 90^o, 270^o and along the wind direction and angle recorded at the nearest weather station for each individual date data was collected. The results were then graphically displayed as separate scatter plots with the convention that negative distances defined are used to denote downwind measurements (right side of the image) and positive distances used to designate upwind locations (left side of the image).

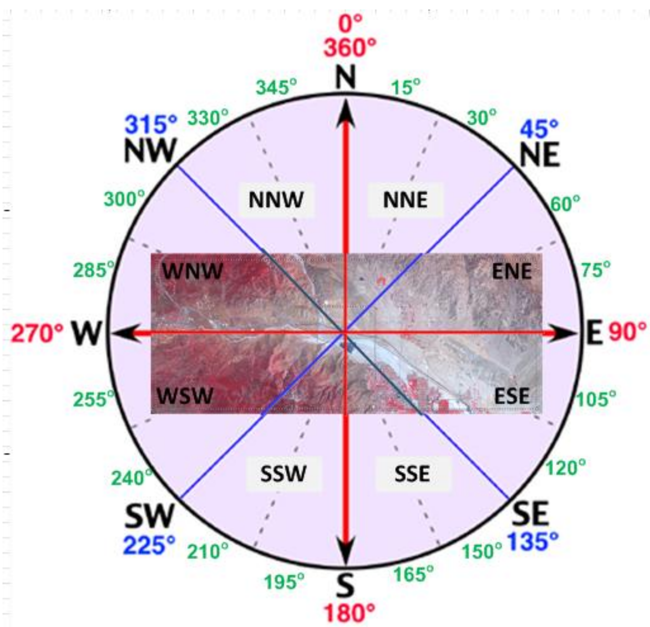

Figure 7. Depiction of the ROI and angles from which temperature values along each line at specified distances were acquired.

An anomaly analysis was examined, however because the temperature values in the data set going true W to E were roughly homogeneous as in the line drawn at 270^{o} elevation was not a factor. Therefore it was found the inclusion of such analysis was not necessary.

Vegetation Analysis Methodology

To analyze any potential effect on or change in vegetation both NDVI and SAVI indices were employed. The analysis incorporating both qualitative and quantitative assessments were completed to determine any change or trend, decrease or increase, in vegetation over 5-year, 10-year, and 20-year periods. The same images identified for the temperature analysis were also used for the requisite vegetation analysis (i.e. same dates, same area and defined boundaries, analysis region is centered on the wind farm, etc.); only the data analysis was altered to specifically analyze potential vegetation change.

Scene Preparation for NDVI Analysis

NDVI for each composite, reprojected image of the region of interest was calculated using the ERDAS NDVI index calculation tool. This built-in function calculates the NDVI values for all pixels in a selected image and produces a grayscale image. This calculation is for a single image and for this analysis; a difference image of NDVI was needed hence a difference image model for NDVI was created (Figure 8). The model uses two input raster images from different dates and subtracts the NDVI values. NDVI difference images were created for every 5, 10 and 20 years within the collected date range of the data set for a total of eight NDVI difference image files. Once all were exported as GeoTIFF files in ERDAS, the actual analysis of the data could be completed both from a quantitative and qualitative perspective using ArcGIS and Excel.

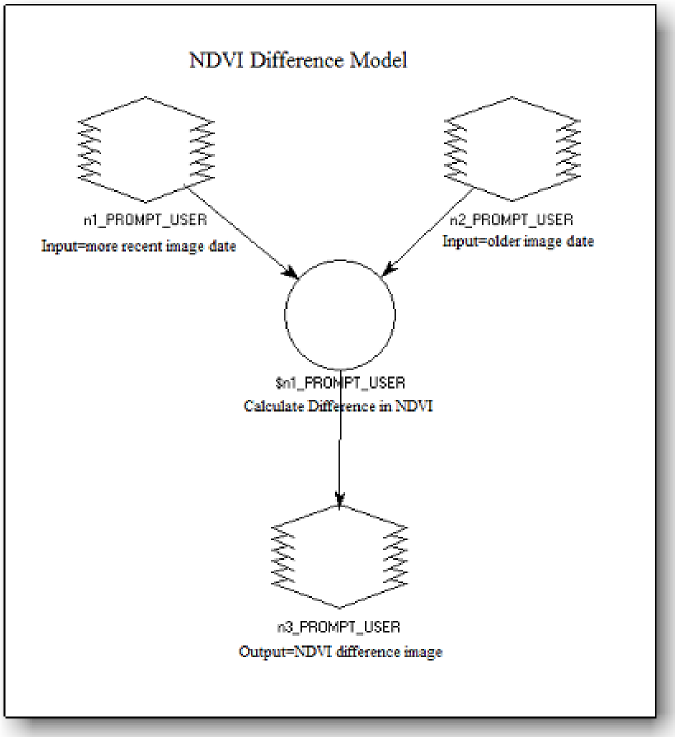

Figure 8. NDVI Difference Model in ERDAS Model Maker.

NDVI Qualitative Analysis

All NDVI difference image pixel values were converted in ArcGIS to integers and displayed using the color scheme where a value of 1 is pink, a value of 0 is grey, and a value of -1 is turquoise. Once displayed in this fashion, direct visual inspection of each difference image was used to empirically determine either a relative gain, loss or no change in vegetation.

NDVI Quantitative Analysis

In ArcGIS, the attribute table was displayed to determine the exact number of pixels that were valued at 1, 0 or -1. These values were then used to create a simple histogram in excel to display the results both visually and quantitatively. The histograms are displayed in the next chapter.

Scene Preparation for SAVI Analysis

The scene preparation for the SAVI analysis was nearly identical to the NDVI preparation; however an additional step was required. As there is no built-in function to calculate SAVI values for a vegetation analysis, a SAVI model using the ERDAS Model Maker was created (Figure 9). The equation for SAVI (Equation 5, Equation 6) was entered in the function circle that is labeled "Calculation of SAVI" (Figure 9) described by the following:

Equation 6. SAVI equation in ERDAS model to calculate SAVI values of images.
((($n1_filename(4)-$n1_filename(3))/($n1_filename(4)+$n1_filename(3)+0.5)) * (1+0.5)).

In this formula, the numeric index 4 refers to band 4 while the numeric index 3 refers to band 3. The value of 0.5 is the constant L which is optimal for a wide range of biomes. For the second SAVI analysis, the constant L was changed to 0.9 as the region is mainly desert and therefore nearly barren.

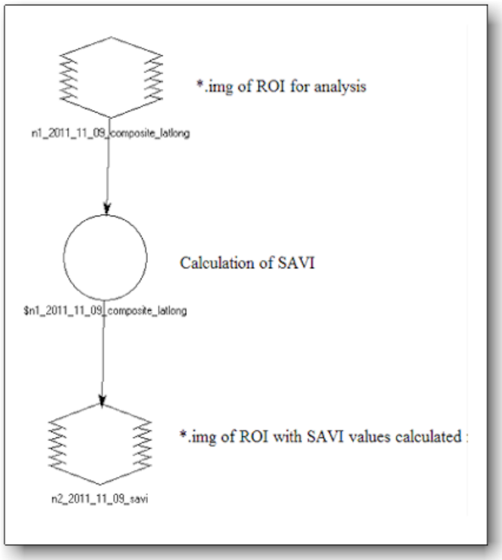

Figure 9. SAVI Calculation Model in ERDAS Model Maker.

The calculation the SAVI model provides the SAVI value for each pixel of a single image and for this analysis, a difference image of SAVI was needed hence a difference image model for SAVI was created (Figure 10). This model was used to determine if there was a difference in vegetation every 5, 10 and 20 years within the date range of the data set. The model uses two input raster images from different dates and subtracts the NDVI values. The SAVI difference model is identical to the NDVI difference model as it subtracts a newer image from an older image, but it uses the SAVI images as opposed to the NDVI images. Again, all were exported as GeoTIFF files in ERDAS and then analyzed both quantitatively and qualitatively using ArcGIS and Excel.

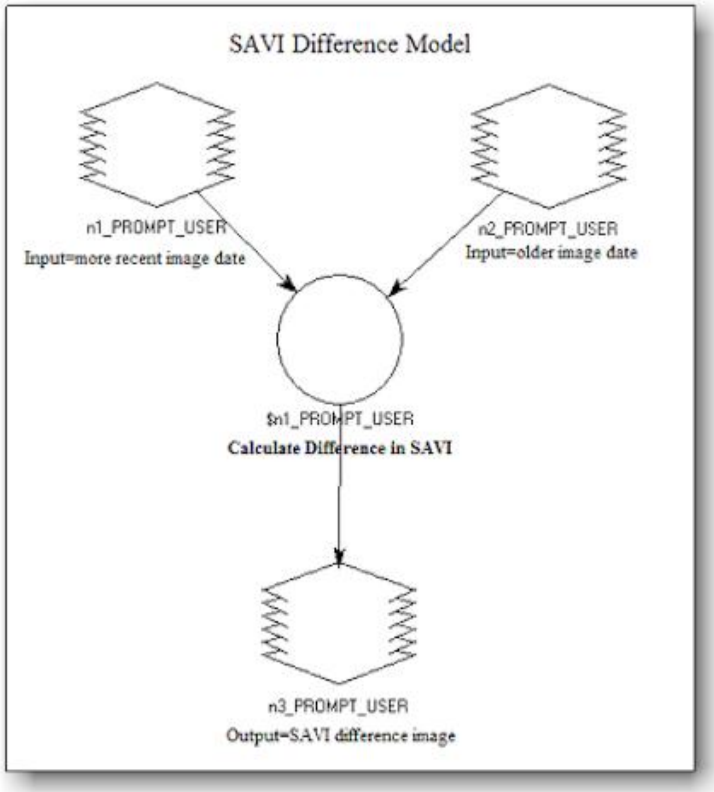

Figure 10. SAVI Difference Model in ERDAS Model Maker.

SAVI Qualitative and Quantitative Analysis

The SAVI qualitative and quantitative analysis followed the same procedure as the previously described NDVI (pages 38) qualitative and quantitative analysis, only of course using the SAVI difference files which were created using the above models. The color scheme used to display the attributes was the same in order for a more direct comparison to be made between the two indices. The results of this analysis are displayed in the Chapter 4.

CHAPTER FOUR: EXPERIMENTS

Impacts on temperature were qualitatively and quantitatively assessed using tools in ERDAS IMAGINE and ArcGIS as well as using R and Excel for the region of interest. A secondary analysis was conducted to determine if an impact on the local vegetation within the region of interest could be observed both qualitatively and quantitatively again using tools in ERDAS IMAGINE and ArcGIS.

Ambient Temperature Analysis

This section defines and discusses the experiments conducted as well as the results obtained which are used to demonstrate the utility of remote sensing imagery and techniques as well as the more generalized quantitative and statistical analysis employed in characterizing the effect of an operational wind farm on ambient temperature. This analysis will be performed in several steps involving the characterization of LST variations surrounding the selected wind farm to assess the contribution of the wind farm itself as well as the ability and potential limitations of remote sensing techniques in identifying these effects.

Qualitative Temperature Assessment

Figure 11 below is a representative example of a thermal-band image showing temperature variation in the region of interest during the winter months. The legend includes ten natural breaks, or subsections, of the temperature range encompassing the entire image calculated and determined in ArcMap. As clearly shown in the legend, the more blue an area is, the cooler the temperatures and conversely the more red an area is, the warmer the temperatures. As indicated in Figure 11, the prevailing wind direction is NNW, which was confirmed by viewing the climatology collected and recorded from a nearby weather station for the particular day and approximate time (October 13, 1984) this image was acquired. Also denoted in the figure below is the San Gorgonio Pass Wind Farm, roughly in the center of the area of interest. In this image, it appears that within the downwind region, South and East of the wind farm, temperatures typically are warmer than those west and north, or mostly upwind, of the wind farm. The areas of blue and green, as well as orange-yellow, both to the North West and almost directly South of the wind farm are mountainous areas and LST values here are largely if not solely attributable to or influenced by the pronounced increase in relative elevation.

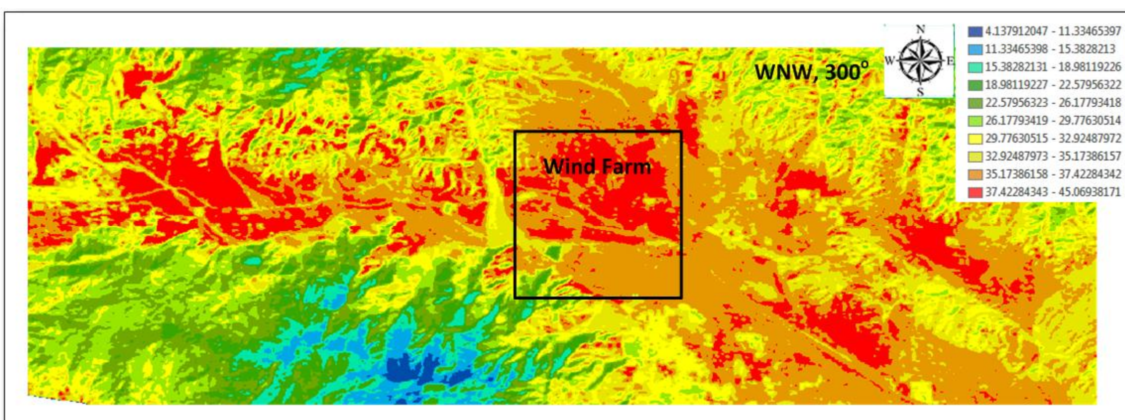

Figure 11. AOI Surface Temperature, Winter.

Overwhelmingly, the winter temperature variation images depict the same characteristics (Figure 12) with one exception of the near-exact opposite temperature variation from a geospatial perspective (Figure 14). In this instance, ground based meteorological data indicates a prevailing wind direction of ESE throughout the day with a change in wind direction approximately at the same time as the image was acquired by the satellite. This observation, as will be discussed later, is particularly striking in that it is at least on initial inspection consistent with the expectation of downwind LST impacts and helps counter the potential argument of a simple northwest to southeast increase in LST. Perhaps the most important observation from this inspection is all twenty-four images were observed to express the same trend of a warming downwind.

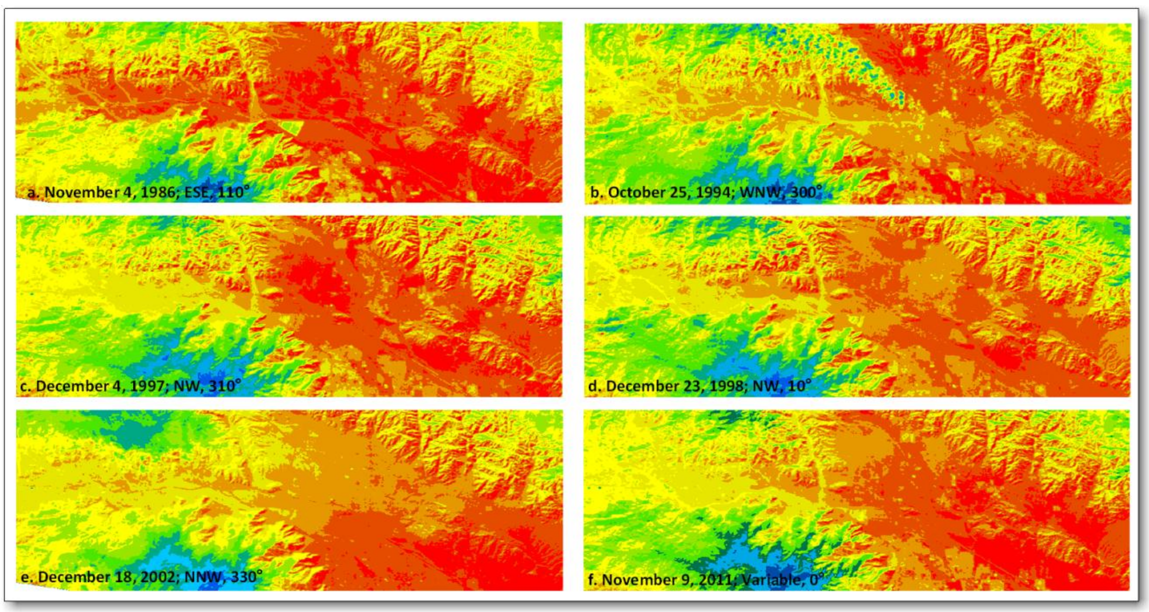

Figure 12. (a.-f.) Subset sample of temperature variation for the area of interest are representative of the majority of winter month images showing the same/similar trend.

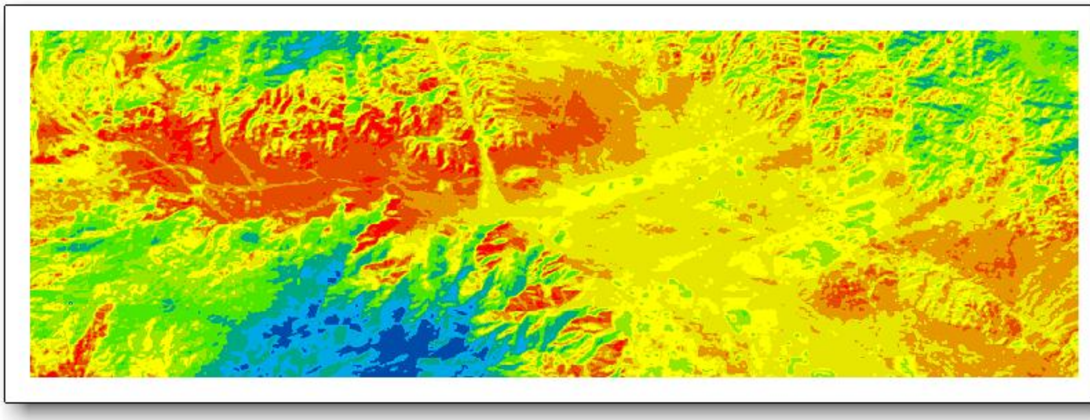

Figure 13. October 30, 1990 depicts the same warming trend as the primary wind direction throughout the day was ESE until the wind direction changed approximately around the time the image was acquired to a WNW direction.

The same analysis was conducted for twenty-seven summer month images. Figure 14 below is an example of temperature variation in the region of interest during summer months. Again, the legend includes ten natural breaks, or subsections, of the temperature range of the entire image calculated and determined in ArcMap. For consistency, the same color palette was chosen and therefore indicates the more blue an area is, the cooler the temperatures and the more red an area is, the warmer the temperatures. Here, the arrows depict the approximate eastward wind direction, which was confirmed by viewing the climatology collected and recorded from a nearby weather station for the particular day (June 18, 2011) and approximate time this image was acquired. Also noted in the figure below is the San Gorgonio Pass Wind Farm, roughly in the center of the area of interest. In this image, it appears the downwind region, south and east of the wind farm, temperatures typically are warmer than those west of the wind farm. As previously noted in the winter month images, the areas of blue and green, as well as orange-yellow, both to the North West and almost directly South of the wind farm, are mountainous areas.

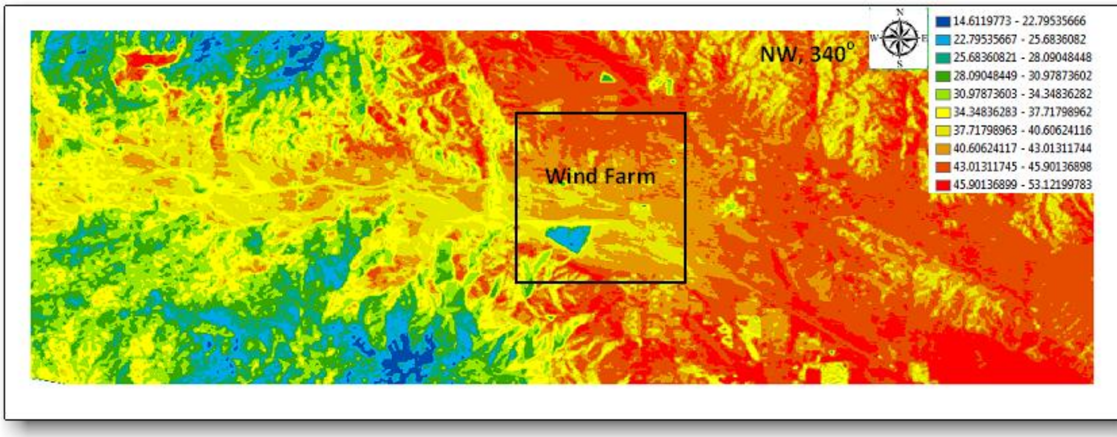

Figure 14. AOI Temperature Variation, Summer.

The summer temperature variation images depict the same characteristics (Figure 15) as observed in the winter images with no exceptions. All twenty-seven images were observed to express the same trend of a marked warming downwind of the wind farm.

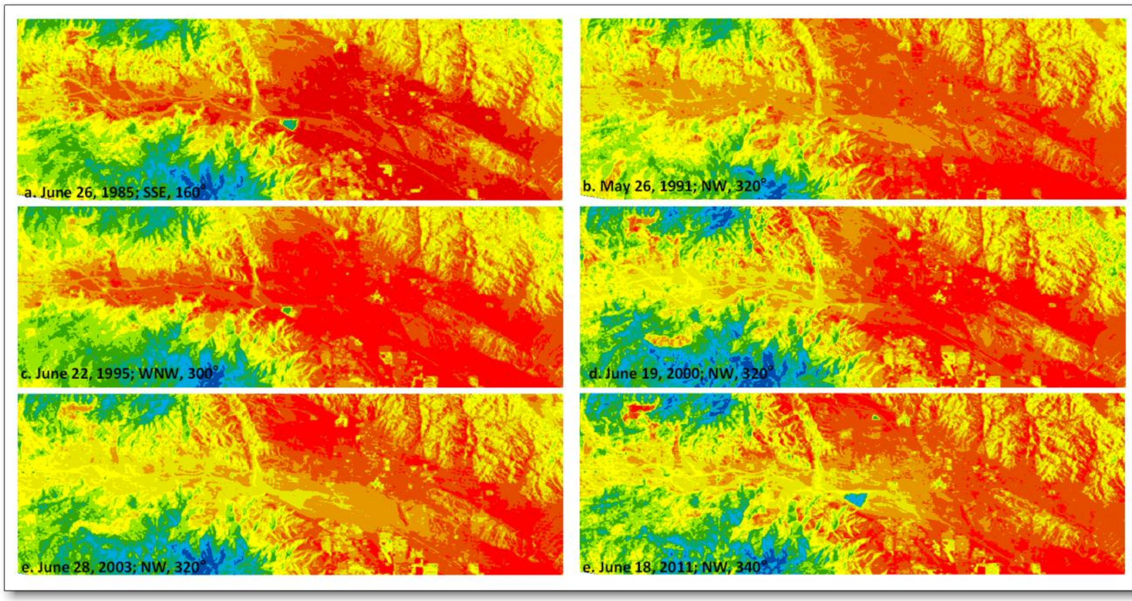

Figure 15. (a.-f.) Subset sample of temperature variation for the area of interest which are representative of the majority of summer month images showing the same/similar trend.

Quantitative Temperature Analysis I

Figure 5 represents the central focus, from a quantitative and statistical analysis perspective, the model derived land surface temperature values in and around the subject wind farm. It will be the primary basis from which to precisely characterize the effect of an operational wind farm on ambient temperature. It is a transformation of the ERDAS, "ASCII" file which simply contains a long linear list of temperature values paired with unique map coordinates to an easier to visualize matrix table format which allows for a more intuitive approach which better links the "Temperature Variation Image Assessment" discussed previously with a quantitative reinforcement of such image based observations.

As described in the methodology chapter, the 2 km x 2 km regions both downwind and upwind were individually averaged to perform the quantitative assessment. In selecting these regions, care was taken to avoid areas comprising significant changes in elevation such as mountains. Figure 16 depicts a sample of winter months and corresponds with the previous qualitative or visual assessment (Figure 12). Consistently it is observed that in the upwind region, average surface temperatures from the upwind boundary of the wind farm through 8 km upwind is cooler than downwind regions from the downwind barrier of the wind farm through 12 km downwind. The standard deviation for the selected regions did not exceed 2^{o}C. The temperature difference between the downwind and upwind regions ranges between approximately two and five degrees warmer downwind than upwind. **This quantitative assessment further supports and is consistent with the results obtained from the qualitative winter month observations.**

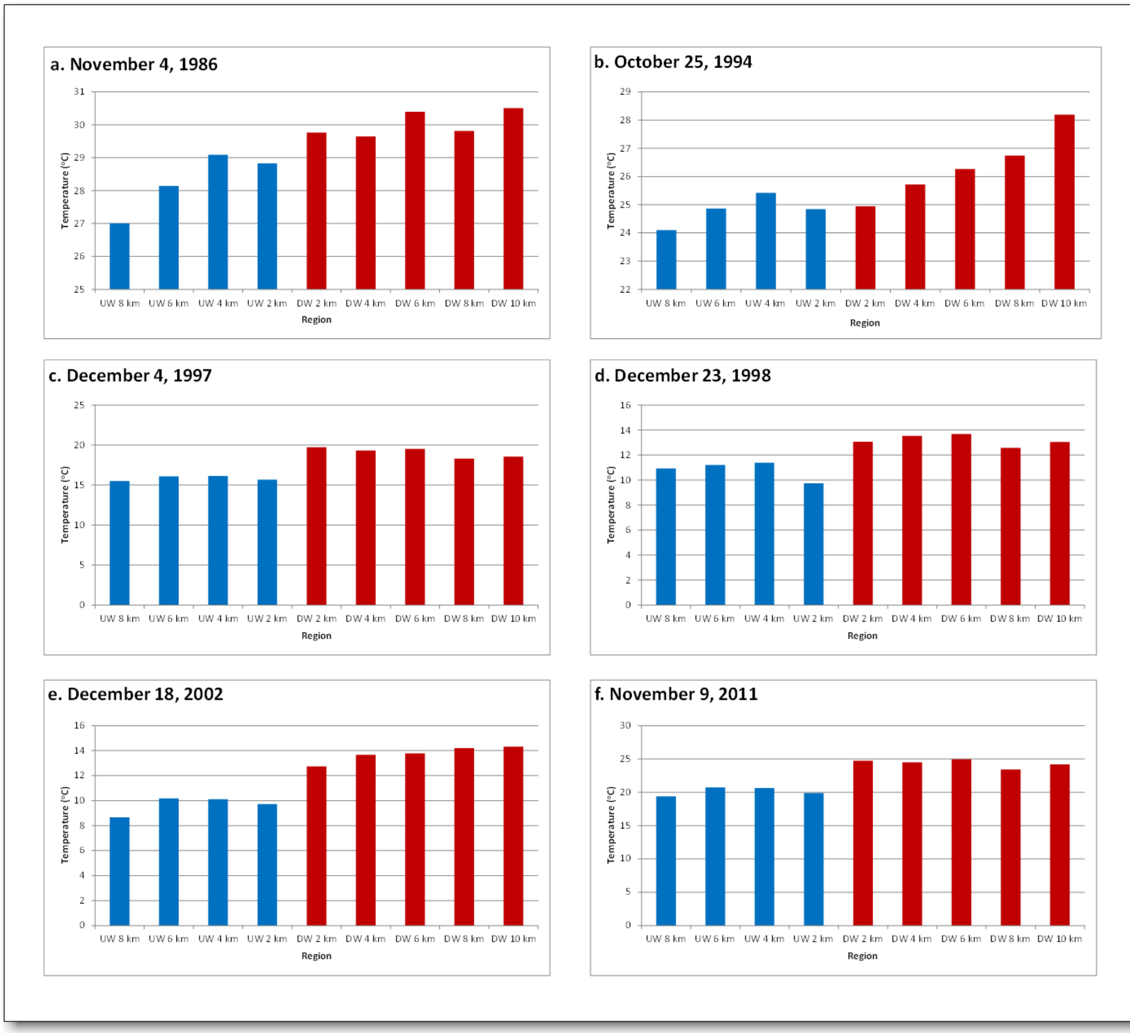

Figure 16. (a.-f.) Comparison of Winter LST from Upwind and Downwind from Wind Farm as a Function of Distance.

Figure 17 is the quantitative analysis which corresponds with Figure 13 above where the same trend was observed where the downwind regions were warmer than the upwind regions but with the wind direction mostly opposite that of the other images examined (ESE vs. WNW).

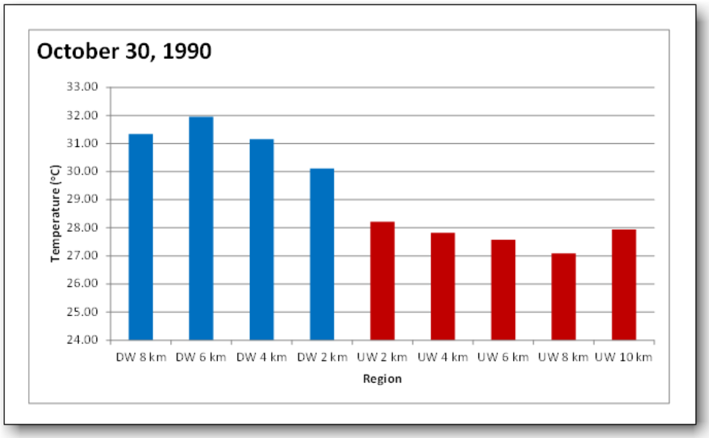

Figure 17. Comparison of LST from Upwind and Downwind from Wind Farm as a Function of Distance from the October 1990 image that depicted the same trend but with wind direction ESE, 135°, throughout the day until the wind direction changed around the time of the image acquisition.

Again, the same quantitative analysis was completed for summer months using 2 km x 2 km regions both downwind and upwind. Figure 18 depicts a sample of summer months and corresponds with the previous qualitative, visual assessment (Figure 15). While it varied how much warmer the downwind regions were, between four and eight degrees, downwind regions through 12 km upwind are shown to be consistently warmer than the observed upwind region through 8 km downwind. The standard deviation for the selected regions did not exceed 2°C. **This quantitative assessment is consistent with the results obtained from the qualitative, visual summer month analysis.**

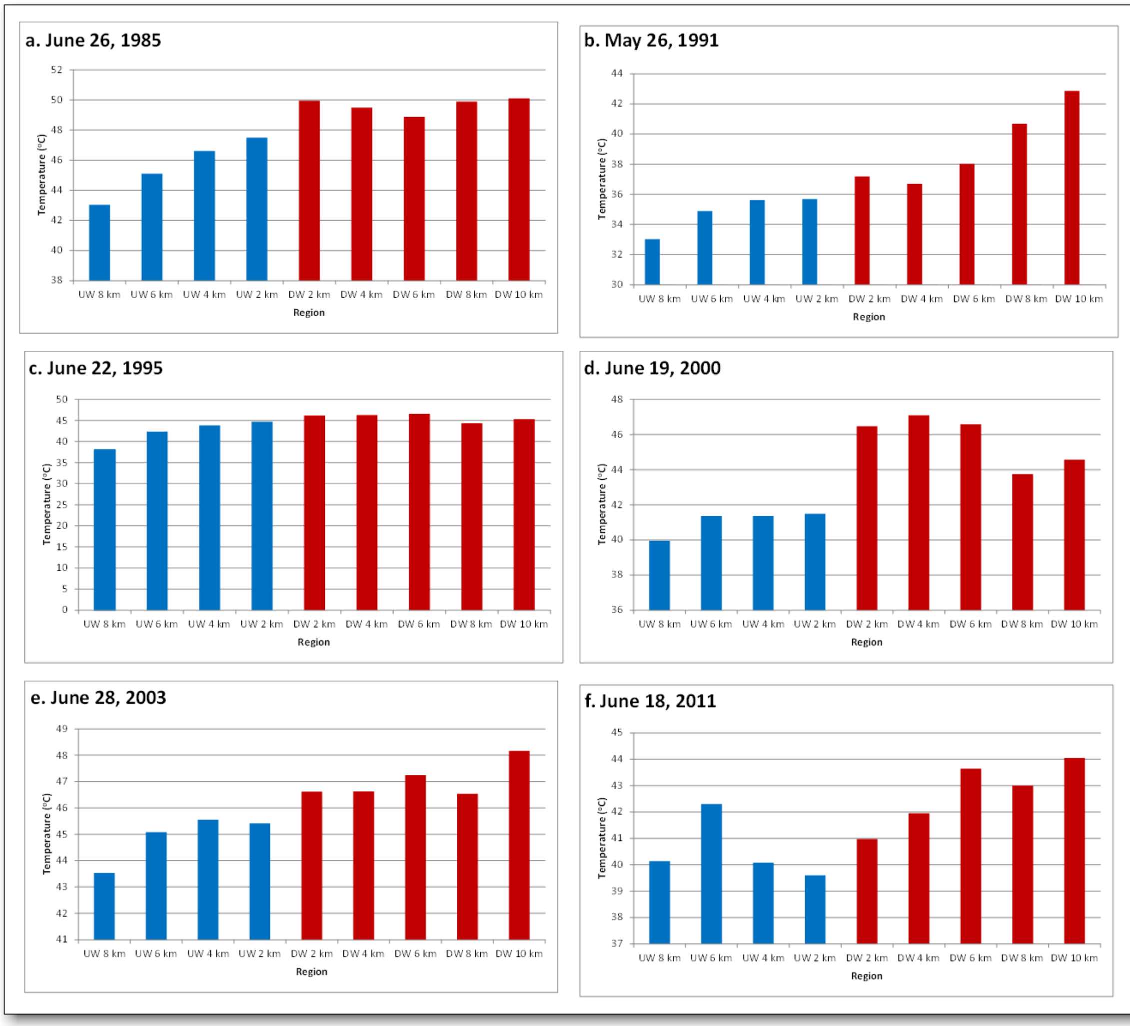

Figure 18. (a.-f.) Comparison of Summer LST from Upwind and Downwind from Wind Farm as a Function of Distance.

Quantitative Temperature Analysis II

The second quantitative temperature analysis was approached by defining specific coordinates at defined distances and angles away from the center of the wind farm. Referencing both the prevailing wind direction for the particular day and the wind direction and angle for the date and approximate time, the results were graphically displayed as scatter plots which predominantly show a warming trend downwind of the wind farm. The scatter plots display either the angles of 75^o, 90^o, and 105^o (E to W) or 255^o, 270^o, and 285^o (W to E) depending upon the prevailing wind direction on the day of image acquisition along with the wind direction and corresponding angle at the approximate time the satellite passed over the ROI.

Figure 19 is representative of the twenty-seven winter images assessed for a recognizable temperature trend. On November 4, 1986 (Figure 19a) the prevailing wind direction for the day was SE while the direction and angle of the wind was ESE, 110^o, hence this was plotted with the angles corresponding to the E to W direction. The temperatures depict a warming trend downwind from the wind farm as the along-wind measurements are progressively higher. For the remaining five scatter plots (Figure 19b-f), the prevailing wind directions were WNW, WNW, NW, NW and W, respectively, and therefore plotted with the angles corresponding to wind directions going from W to E. Here to, it is observed that the downwind LST values are distinctly warmer than the corresponding upwind data points. While the wind direction angles varied to some extent, they too show the same warming trend downwind of the wind farm. **These results correlate well with and are in agreement with the first quantitative analysis discussed above.**

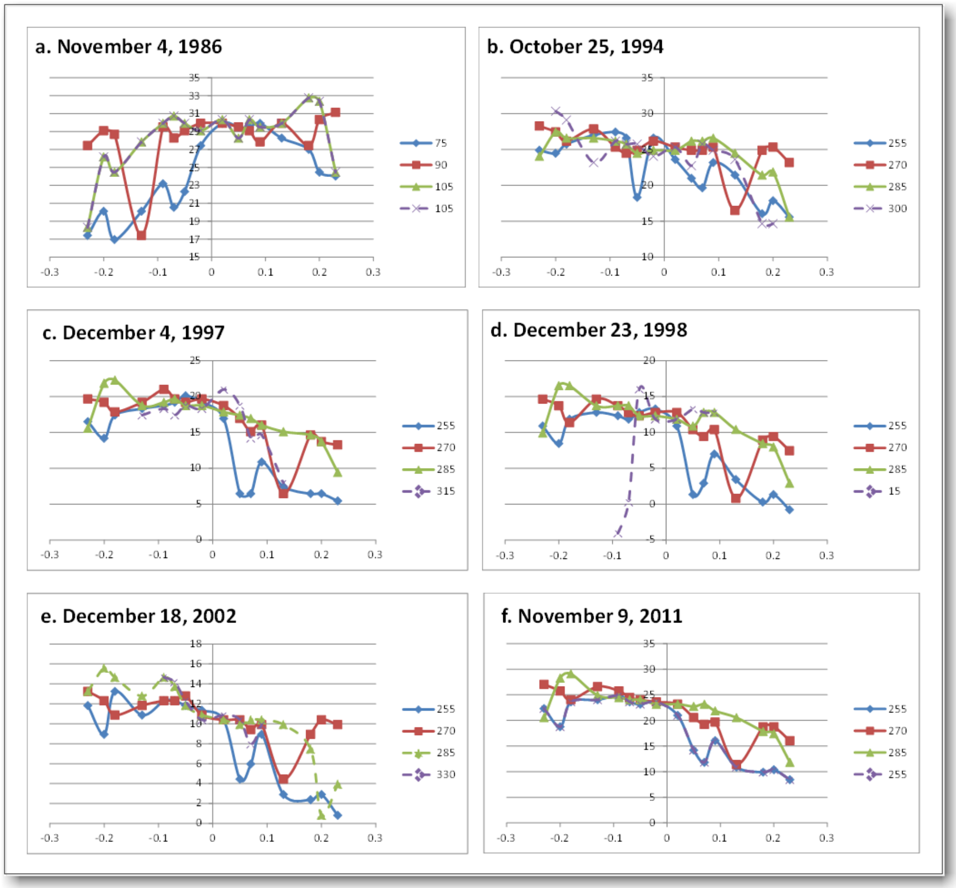

Figure 19. (a.-f.) Winter months. In each of the scatter plot the x-axis is representative of the distance from the center of the wind farm with negative numbers corresponding to the right half of the image displayed in Figure 12 and the positive numbers corresponding to the left half of the images displayed in Figure 12. The y-axis is temperature in degrees Celsius. The fourth series listed in each of the legends is representative of the wind direction and angle according to a nearby weather station.

An identical analysis was conducted for the summer months in which Figure 20 is representative of the twenty-eight images assessed during this seasonal period. Again it is observed that the downwind areas of the wind farm are consistently warmer than the areas upwind when plotted against the angles corresponding with the E to W direction. Again, in the remaining five scatter plots (Figure 20b-f) all exhibited similar wind directions of WNW, W, NW, NW, and NNW, respectively and were plotted with the angles corresponding to wind directions going from W to E. It is again observed that the downwind temperature values are consistently and predominantly warmer than the associated upwind measurements. While the wind direction angles varied, they too show the same warming trend downwind of the wind farm. **Again as previously shown for the winter months, these results correlate well with the first quantitative analysis above.**

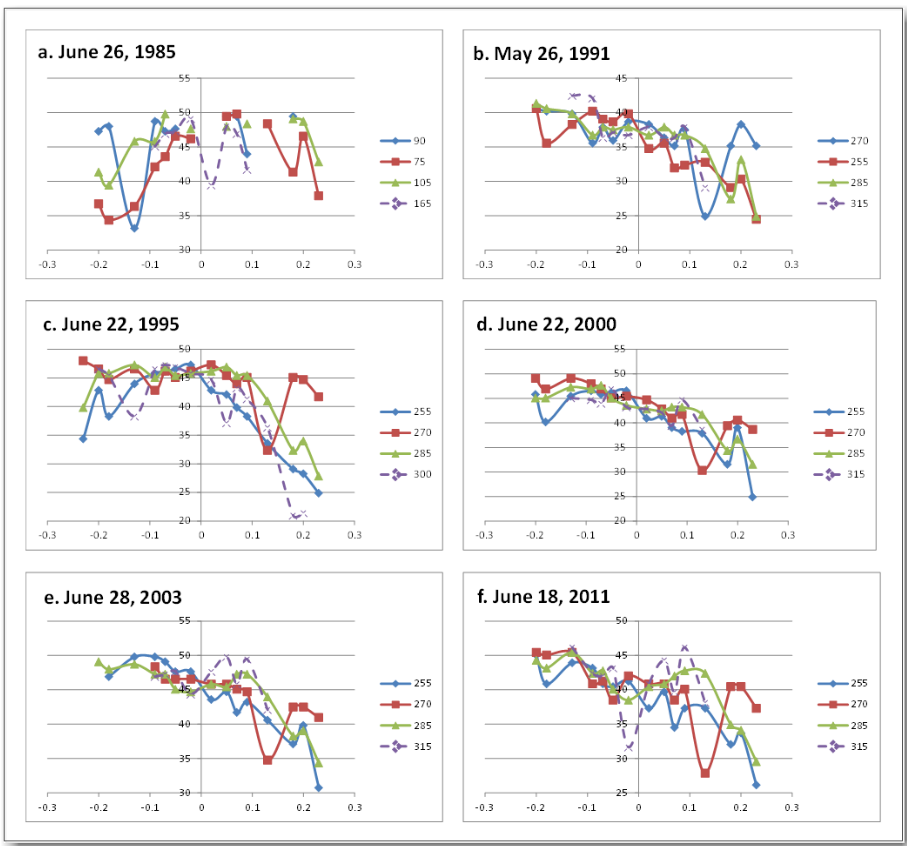

Figure 20. (a.-f.) Summer months. In each of the scatter plot the x-axis is representative of the distance from the center of the wind farm with negative numbers corresponding to the right half of the image displayed in Figure 15 **a**nd the positive numbers corresponding to the left half of the images displayed in Figure 15. The y-axis is temperature in degrees Celsius. The fourth series listed in each of the legends is representative of the wind direction and angle according to a nearby weather station.

Vegetation Experiments

This section defines and discusses the experiments conducted as well as the results obtained which are used to demonstrate the utility of remote sensing imagery and techniques as well as the more generalized quantitative and statistical analysis employed in characterizing the effect of an operational wind farm on vegetation of the region of interest using the two indices, NDVI and SAVI. This analysis includes both qualitative and quantitative assessments of vegetation changes over 5-year, 10-year, and 20-year periods.

NDVI Vegetation Qualitative Assessment

Figure 21 below depicts 5-year, 10-year, and 20-year NDVI difference images for the summer months. As denoted in the legend, a value of -1 (pink) indicates a loss of vegetation while a value of 1 (turquoise) indicates an increase in vegetation. A value of 0 (grey) indicates no change in vegetation and it is the attribute that dominates the region of interest. Here it is clear there is limited vegetation detected in both the desert mountain pass and areas surrounding the wind farm. However, areas of change in vegetation have been detected in locations southeast of the wind farm due to primarily if not solely to increases in urbanization, while in the mountainous areas in the western portion of the image, there is detectable vegetation using NDVI primarily due to elevation related changes in environment which naturally contribute to relative abundance of same. Nearly identical results have been observed for the winter months as well.

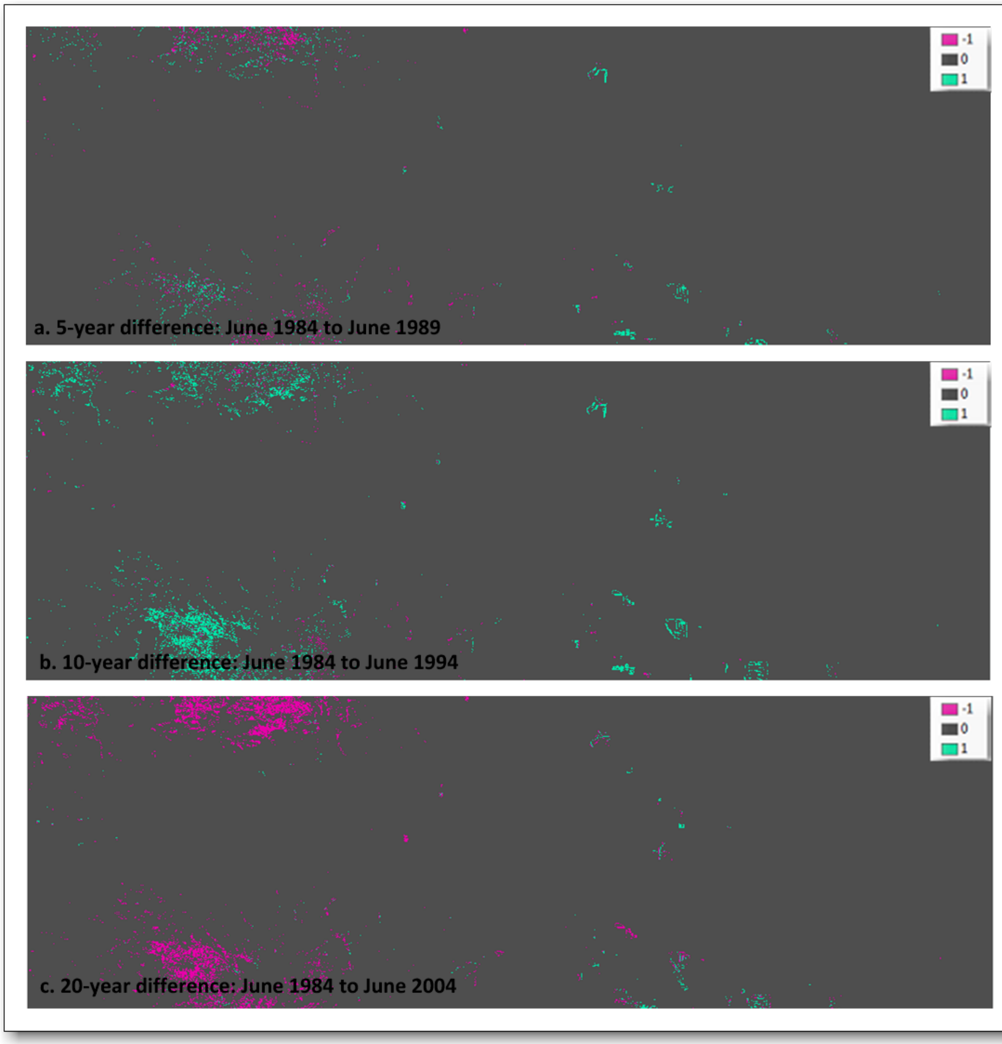

Figure 21. Samples of NDVI difference (a) 5-year difference, (b) 10-year difference, and (c) 20-year difference.

NDVI Vegetation Quantitative Assessment

For each NDVI difference calculation, a histogram was created to quantitatively display the change in vegetation in both summer and winter months at intervals of every five, ten and twenty years. Figure 22 is a representative example of such results, with little variation observed between summer and winter across each of the specified different time frames. **All histogram summaries show that overall there was no significant**

change in vegetation for the region of interest as represented in the grey bar denoting, the number of pixels from which a NDVI difference value of zero was derived.

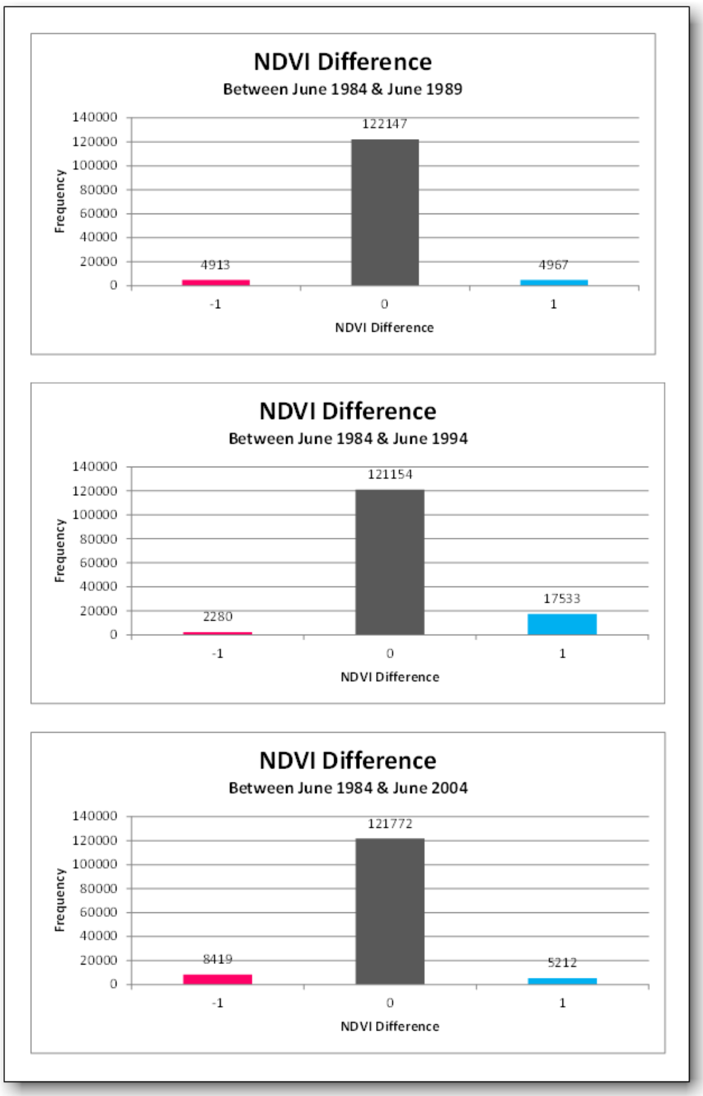

Figure 22. Sample of summer histograms of NDVI difference images: (a) 5-year, (b) 10-year and (c) 20-year.

SAVI Vegetation Qualitative Assessment

Figure 23 below depicts a sample of 5-year, 10-year, and 20-year SAVI difference (L = 0.5) images for the summer months. As denoted in the legend, a value of -1(pink) indicates a loss of vegetation while a value of 1(turquoise) indicates an increase in vegetation. A value of 0 (grey) indicates no change in vegetation and it is the attribute that dominates the region of interest. From a qualitative and superficial visual perspective, using 0.5 for the soil-brightness correction factor in the SAVI equation shows there is nearly no observably significant change in vegetation in the entire image for both the summer and winter months.

Figure 23. Samples of SAVI difference (L=0.5) (a) 5-year difference, (b) 10-year difference, and (c) 20-year difference.

Figure 24 below depicts 5-year, 10-year, and 20-year SAVI difference (L = 0.9) images for the summer months. The same legend has been used for consistency for the comparative analysis. Using the soil brightness correction factor of 0.9 shows results consistent with the NDVI analysis. However, some of the gains and losses of vegetation in the desert pass is slightly more noticeable from a visual perspective. Similar to the NDVI analysis, the changes over time in the mountain regions and urbanized areas are also detectable. Nearly identical results have been observed for the winter months as well.

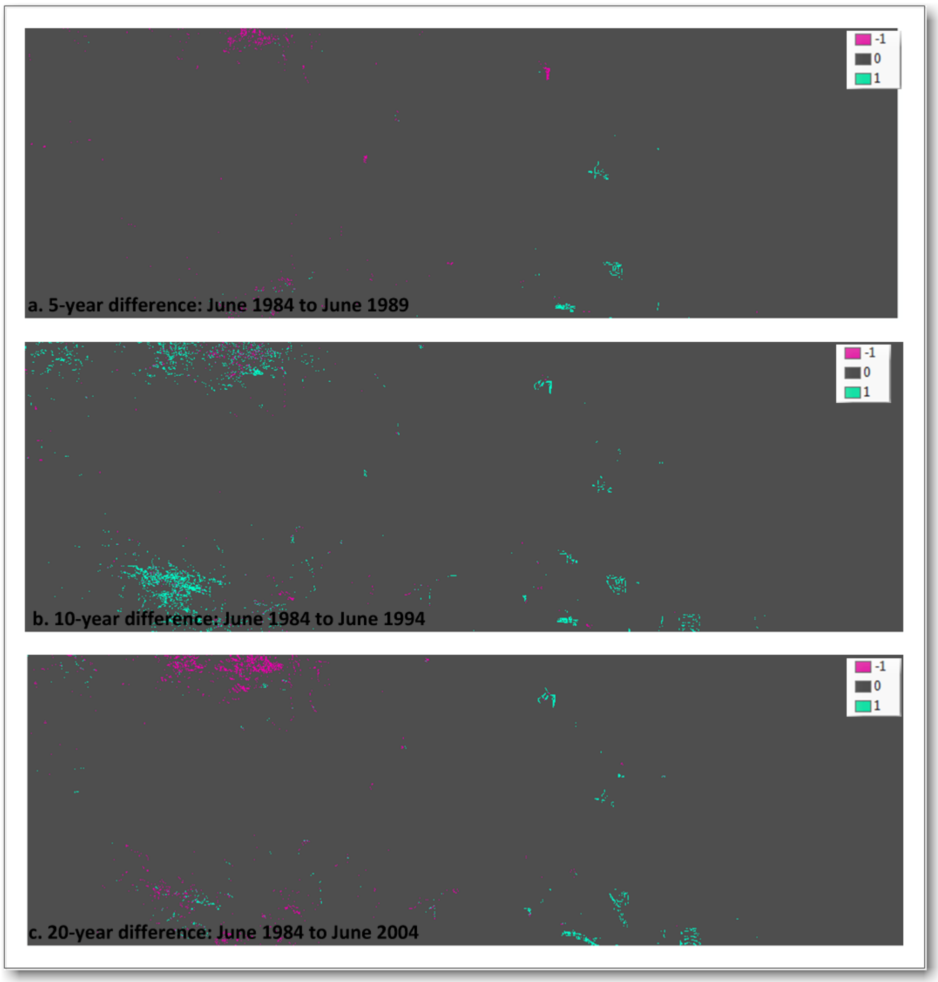

Figure 24. Samples of SAVI difference (L=0.9) (a) 5-year difference, (b) 10-year difference, and (c) 20-year difference.

SAVI Vegetation Quantitative Assessment

For each SAVI difference (L = 0.5) calculation, a histogram was created to quantitatively display the change in vegetation for both summer and winter months at intervals of every five, ten and twenty years. Figure 25 is a representative example of results, with little variation resulting between summer and winter across each of the specified different time frames. All histogram summaries show that overall there was even less change detected using the soil brightness correction factor of 0.5 when compared to the NDVI results. **The histograms show an extremely minimal change in vegetation as represented in the grey bar, the number of pixels from which a NDVI difference value of zero was derived.**

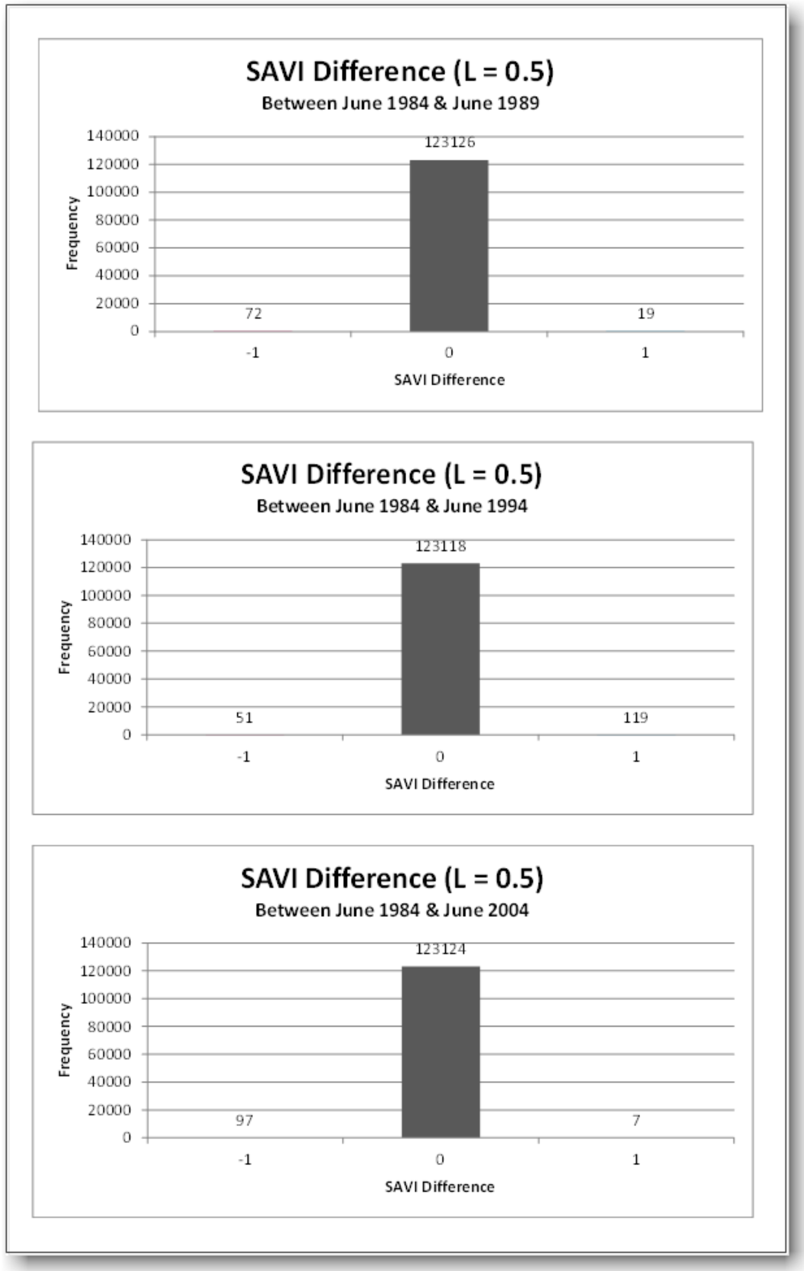

Figure 25. Sample of summer histograms of SAVI difference (L = 0.5) images: (a) 5-year, (b) 10-year and (c) 20-year.

For each SAVI difference (L = 0.9) calculation, a histogram was also created to quantitatively display the change in vegetation in both summer and winter months at intervals of every five, ten and twenty years. Figure 26 is a representative example of such results, with slight variation resulting between summer and winter across each of the specified different time frames. All histogram summaries show that overall there was no change in vegetation for the region of interest as represented in the grey bar denoting the number of pixels from which a NDVI difference value of zero was derived. However, with the soil brightness correction factor of 0.9, there is a more notable number of pixels where there are areas of loss and gain in vegetation unlike in the NDVI analysis and the SAVI ($L = 0.5$) analysis. This loss and gain in vegetation however is still primarily observed in the mountainous and urbanized zones of the region of interest.

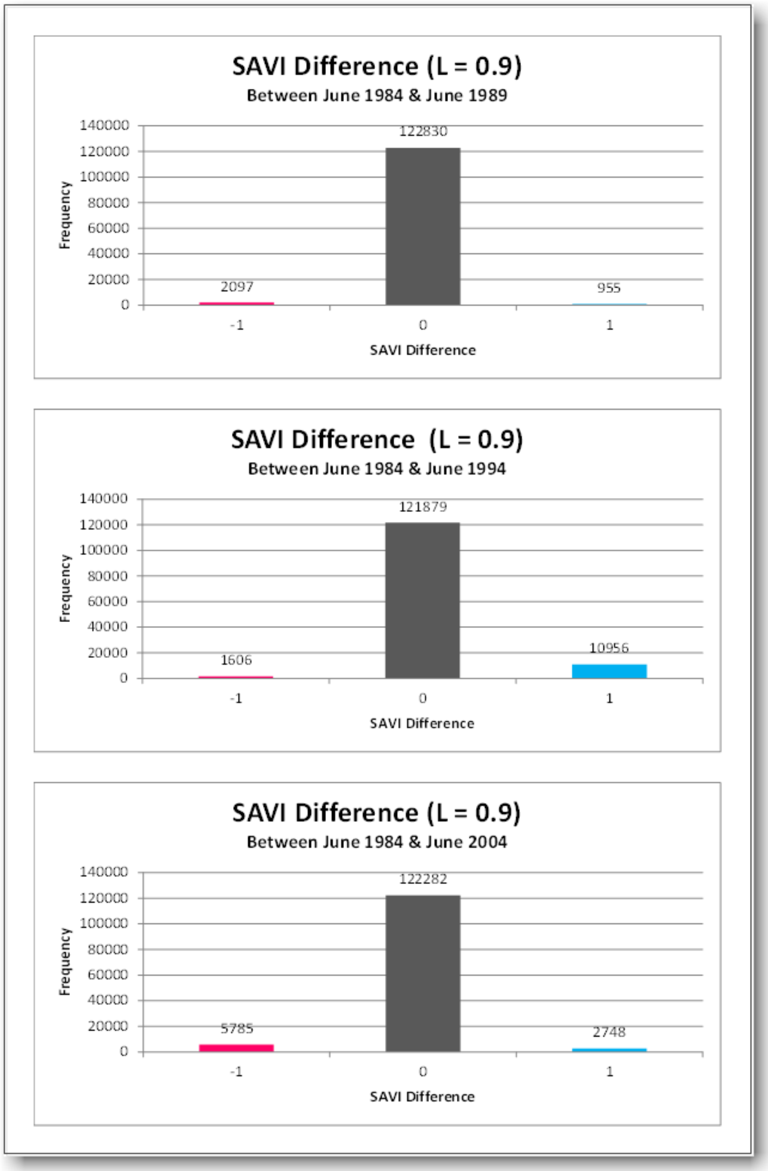

Figure 26. Sample of summer histograms of SAVI difference (L = 0.9) images: (a) 5-year, (b) 10-year and (c) 20-year.

CHAPTER FIVE: CONCLUSION

The harnessing of wind power is a vital and increasingly dominant component to satisfy our energy needs while minimizing the use of fossil fuels. It is rapidly becoming the main resource for decreasing the dependency on coal, oil and natural gas. With the increase in both the number and scale of wind farms for this purpose, it is essential that we continue to build on our understanding of both the costs and benefits of wind energy at many levels, especially concerning environmental impacts of such installations and this thesis defines and utilizes a set of cost effective techniques which contributes to this effort. While there are numerous studies which have examined various categories of impacts to our environment as a result of wind farm use, this thesis has sought to extend the use of satellite based remote sensing in conjunction with accepted methodologies to provide clearer insight into the effects of large scale wind farms on land surface temperature. Perhaps most importantly, this effort suggests a path forward for expanding such analytical assessment on a larger scale.

One of the most significant aspect of this thesis was the demonstration that remote sensing imagery could be effectively used in conjunction with off the shelf software to analyze and explore the impacts of a large scale wind farm on the local environment, more specifically in terms of land surface temperature. Freely available Landsat 5 TM scenes were selected and processed using an accepted model based approach for determining land surface temperature values in the vicinity surrounding and within a large scale wind farm. With the region of interest defined, the area was analyzed both from a qualitative and quantitative perspective to identify and characterize an observable warming trend downwind of the wind farm as modeled in previous studies. The experimental analysis correlated well with similar warming trends that were simulated in as well as measured albeit a much smaller, land based scale as previously cited herein.

Can remote sensing imagery and techniques show that wind farms affect near-surface air temperatures?

Through the experiments conducted and the results presented in this thesis, it is clear that satellite-based remote sensing techniques can make an effective contribution towards and have a significant value in studying the impacts of wind farms on the environment. In particular, addressing the effects on land surface temperature through the use of satellite imagery was demonstrated from both qualitative and quantitative perspectives. The qualitative image analysis which involved a visual inspection of the region of interest using color keyed land surface temperature patterns revealed distinct variations in temperature both upwind and downwind of the wind farm exhibiting warmer temperatures appearing predominantly downwind. **Through two separate quantitative analyses, the visual or qualitative assessment was confirmed demonstrating the same results graphically in conjunction with the display of local meteorological wind data. The remote sensing imagery and analysis approach has shown to be readily effective in the quantitative characterization of a large scale wind farm's influence on temperature.**

Can remote sensing further validate the model simulation findings of previous studies?

The subsequent analysis of the collected remote sensing imagery empirically supports the predictions of existing computer based models which identifies a warming temperature trend downwind of a wind farm as well as the brief period of meteorological campaign data near the San Gorgonio Pass Wind Farm, a particularly expansive wind farm in California. The eddies that are created by a wind farm result in enhanced vertical mixing with the local atmosphere leading to the observation of a warming of surface temperature which was primarily seen during nighttime hours and into the early morning. The imagery acquired for this thesis was captured by the Landsat 5 satellite in the evening and the resulting temperature trend showing a warming downwind of the wind farm as seen in both the qualitative and quantitative analysis correlates well with the findings of the computer models and the relatively small amount of meteorological campaign data that is available. **Not only does this thesis support and validate the model simulation findings of previous studies it does so in a significant and convincing way by incorporating very large datasets acquired over a number of years during which the subject wind farm has been in operation. In addition these large datasets have been analyzed using proven methodology that has been focused on the effort to validate these models which adds further credibility to the supporting the findings.**

Can remote sensing techniques further explore/detect trends of other [potential] impacts of wind farms such as a change in local precipitation or vegetation?

As a secondary analysis, well accepted vegetation indices were additional environmental variable examined for this thesis. While small changes in vegetation were detected in the higher elevations of the region of interest, a conclusion regarding whether the wind farm played a role in this change cannot be made. In the areas that perhaps a more direct effect on vegetation may be expected to occur due to the wind farm, there is limited to no vegetation as the region is part of the Mojave Desert where vegetation is sparse. **This is not to say that vegetation is not effected by a large scale wind farm.** Remote sensing techniques have the capability of providing data from which to further explore and detect potential impacts of wind farms on vegetation, however, this region is not ideal for such analysis. While through the use of vegetation indices such as the ones described in this thesis, NDVI and SAVI, such assessment of a trend in vegetation change can be analyzed. **However the current study within this thesis was of minimal value due to the desert environment in which the region of interest was situated and no definitive conclusion can be drawn regarding impacts to local vegetation.**

Suggested Future Research

For future studies it would be ideal to use remote sensing techniques in conjunction with field data as well as more advanced numerical and computer models which would produce sound, proper and very valuable environmental assessments of the placement, construction and operation of wind farms. Additionally, conducting the same or similar analysis for other large scale wind farms would be of interest and importance for several reasons. For other large wind farms not sited in desert biomes, in addition to temperature, a more in depth and useful analysis regarding influences on vegetation would be possible as these other wind farms are likely contain more substantial vegetation. Impact on local precipitation is another potential variable that would have been difficult to evaluate in a desert region and therefore study of a large scale wind farm located in a different climatic zone in which precipitation is a more significant component would be more applicable. Effects of wind farm operation on precipitation have also been modeled with computer-based simulations in a manner similar to that done for LST and therefore an analogous study as employed in this thesis using remote sensing techniques to assess precipitation effects would be of value to validate such model predictions.

A final recommendation for future study incorporates an analysis over a greater time scale which would assess changes in environmental variables both before and after installation and operation. Such an analysis would require remote sensing data to be readily available for a significant time period, about 5-10 years, before the wind farm was operational in order for a comparison to be made.

Most research regarding environmental effects on wind farms involve the effects on a global scale or on avian and aesthetic impacts on a local scale. This thesis along with other current research regarding local environmental effects provide a more realistic and precise estimate of the impacts large scale wind farms have on the local environment. The experiments conducted have addressed the effects on temperature as well as have attempted to address effects on vegetation at a local level using remote sensing data. This research has been done in a successful effort to better understand and acknowledge what impact current wind energy technology has on the environment as well as to support and encourage the improvement of wind energy technologies to be more sustainable and to better improve the environment in which we live.

REFERENCES

REFERENCES

Baidya Roy, S. (2011). Simulating impacts of wind farms on local hydrometeorology. Journal of Wind Engineering and Industrial Aerodynamics, 99, 491-498.

Baidya Roy, S., Pacala, S., & Walko, R. (2004). Can large wind farms affect local meteorology? *J. Geophys. Res*, *109*, D19101.

Baidya Roy, S., & Traiteur, J. J. (2010). Impacts of wind farms on surface air temperatures. *Proceedings of the National Academy of Sciences*, *107*(42), 17899–17904.

California Department of Fish and Game. (2003). *Atlas of the Biodiversity of California* (1st ed.). In E. Kauffman (Eds.), *Climate and Topography* (pp. 12-15). Sacramento, CA.

Campbell, J. B. (2006). *Introduction to Remote Sensing, Fourth Edition* (4th ed.). The Guilford Press.

Krewitt, W., & Nitsch, J. (2003). The potential for electricity generation from on-shore wind energy under the constraints of nature conservation: a case study for two regions in Germany. *Renewable energy*, *28*(10), 1645–1655.

Department of the Interior U.S. Geological Survey. (2009). *Landsat Thematic Mapper (TM) Level 1 (L1) Data Format Control Book (DFCB)*. Retrieved January 5, 2012, from http://landsat.usgs.gov/documents/LS_DFCB_20_TM_Level_1_DFCB.pdf.

Desholm, M., Fox, A., Beasley, P., & Kahlert, J. (2006). Remote techniques for counting and estimating the number of bird–wind turbine collisions at sea: a review. *Ibis*, *148*, 76–89.

Drewitt, A. L., & Langston, R. H. W. (2006). Assessing the impacts of wind farms on birds. *Ibis*, *148*, 29–42.

Elmore, A. J., Mustard, J. F., Manning, S. J., & Lobell, D. B. (2000). Quantifying vegetation change in semiarid environments: precision and accuracy of spectral mixture analysis and the normalized difference vegetation index. *Remote Sensing of Environment*, *73*(1), 87–102.

Global Wind Energy Council. (2011). Global Wind Report: Annual market update 2010. In GWEC publications. Retrieved January 28, 2012, from http://www.gwec.net/fileadmin/images/Publications/GWEC_annual_market_update_2010_-_2nd_edition_April_2011.pdf

Huete, A. (1988). A soil-adjusted vegetation index (SAVI). *Remote sensing of environment*, *25*(3), 295–309.

Huete, A., & Warrick, A. (1990). Assessment of vegetation and soil water regimes in partial canopies with optical remotely sensed data. *Remote sensing of environment*, *32*(2-3), 155–167.

Holtzclaw, K. M. (2006). *San Gorgonio Pass (CA)*. Arcadia Publishing.

Keith, D. W., DeCarolis, J. F., Denkenberger, D. C., Lenschow, D. H., Malyshev, S. L., Pacala, S., & Rasch, P. J. (2004). The influence of large-scale wind power on global climate. *Proceedings of the National Academy of Sciences of the United States of America*, *101*(46), 16115.

National Park Service. (2006). *Mojave Desert*. Retrieved February 16, 2012, from http://www.nps.gov/jotr/naturescience/mojave.htm.

Qin, Z., Karnieli, A., & Berliner, P. (2001). A mono-window algorithm for retrieving land surface temperature from Landsat TM data and its application to the Israel-Egypt border region. *International Journal of Remote Sensing*, *22*(18), 3719–3746.

Sobrino, J. A., Jimenez-Munoz, J. C., & Paolini, L. (2004). Land surface temperature retrieval from LANDSAT TM 5. *Remote Sensing of Environment*, *90*(4), 434–440.

Sta Maria, M. R., & Jacobson, M. Z. (2009). Investigating the effect of large wind farms on energy in the atmosphere. *Energies*, *2*(4), 816–838.

Sun, Q., Tan, J., & Xu, Y. (2010). An ERDAS image processing method for retrieving LST and describing urban heat evolution: a case study in the Pearl River Delta Region in South China. *Environmental Earth Sciences*, *59*(5), 1047–1055.

U.S. Department of the Interior. (2008). *Right-of-Way (R/W) Grant CACA-11688-A Mesa Wind Power Corporation.* (DOI-BLM-CA-060-0007-0057-EA). Palm Springs, CA: Author. Retrieved from http://www.blm.gov/pgdata/etc/medialib/blm/ca/pdf/palmsprings/general_-_pssc.Par.52889.File.dat/07-57%20Mesa%20Wind%20EA%20Final%206-12.pdf

Wang, L. T., & De Liberty, T. L. (2005). Landsat Atmospheric Correction: The Good, the Bad, and the Ugly. *University of Delaware, Department of Geography, USA. gis. esri. com/library/userconf/proc05/papers/pap1560. pdf (14.05. 2008).*

Wiser, R. et al. (2007). *Annual Report on US Wind Power Installation, Costs, and Performance Trends: 2006.* (US Dept of Energy), Washington, D.C.: Author. Retrieved from http://www.nrel.gov/docs/fy07osti/41435.pdf

CURRICULUM VITAE

Jenell M. Walsh-Thomas graduated from Lenape High School, Medford, New Jersey, in 2006. She received her Bachelor of Science in Environmental Science and Policy from Marist College in 2010.